Universal transport near a quantum critical Mott transition in two dimensions

William Witczak-Krempa,[1] Pouyan Ghaemi,[2] T. Senthil,[3] and Yong Baek Kim[1,4]
[1]*Department of Physics, University of Toronto, Toronto, Ontario, Canada M5S 1A7*
[2]*Department of Physics, University of Illinois at Urbana-Champaign, Urbana, Illinois 61801-3080, USA*
[3]*Department of Physics, Massachusetts Institute of Technology, Cambridge, Massachusetts 02139, USA*
[4]*School of Physics, Korea Institute for Advanced Study, Seoul 130-722, Korea*
(Received 19 July 2012; published 5 December 2012)

We discuss the universal-transport signatures near a zero-temperature *continuous* Mott transition between a Fermi liquid and a quantum spin liquid in two spatial dimensions. The correlation-driven transition occurs at fixed filling and involves fractionalization of the electron: upon entering the spin liquid, a Fermi surface of neutral spinons coupled to an internal gauge field emerges. We present a controlled calculation of the value of the zero-temperature universal resistivity jump predicted to occur at the transition. More generally, the behavior of the universal scaling function that collapses the temperature- and pressure-dependent resistivity is derived, and is shown to bear a strong imprint of the emergent gauge fluctuations. We further predict a universal jump of the thermal conductivity across the Mott transition, which derives from the breaking of conformal invariance by the damped gauge field, and leads to a violation of the Wiedemann-Franz law in the quantum critical region. A connection to the quasitriangular organic salts is made, where such a transition might occur. Finally, we present some transport results for the pure rotor $O(N)$ conformal field theory.

DOI: 10.1103/PhysRevB.86.245102 PACS number(s): 71.10.Hf, 71.30.+h, 75.10.Kt, 71.27.+a

I. INTRODUCTION

Despite decades of study, the Mott metal-insulator transition remains a central problem in quantum many-body physics.[1] In recent years attention has refocused on an old question: Can the Mott transition at $T = 0$ be continuous? Usually, the Mott insulating state also has magnetic long-range order or in some cases broken lattice symmetry which doubles the unit cell. In such situations, a continuous Mott transition between a symmetry-unbroken metal and the Mott insulator requires not just the continuous onset of the broken symmetry, but also the continuous destruction of the metallic Fermi surface. It is currently not clear theoretically if such a continuous quantum phase transition can ever occur.

Considerable theoretical progress[2–8] has been possible in situations in which the Mott insulator does not break any symmetries but rather is in a quantum spin-liquid (SL) state.[9] The evolution from the Fermi-liquid (FL) metal to the quantum spin-liquid state is of interest because it provides an opportunity to understand the fundamental phenomenon of the metal-insulator transition (MIT) without the complications of the interplay with the onset of broken symmetry. Such a transition has acquired experimental relevance with the discovery of quantum spin-liquid Mott insulators near the Mott transition in a few different materials, notably the quasi–two-dimensional triangular lattice organic salts[10–15] κ-(BEDT-TTF)$_2$Cu$_2$(CN)$_3$ and EtMe$_3$Sb[Pd(dmit)$_2$]$_2$, and the three-dimensional hyper-kagome material[16] Na$_4$Ir$_3$O$_8$. Indeed, upon application of hydrostatic pressure, these quantum spin liquids become metallic.[17] [The phase diagram of κ-(BEDT-TTF)$_2$Cu$_2$(CN)$_3$ in addition has superconductivity at lower temperatures.] The nature of the transition in the experiments is not currently understood but could be potentially described by a SL-FL quantum critical MIT.

A wide variety of quantum spin-liquid phases can exist theoretically. However, a natural state[3,18,19] that emerges near the Mott transition is a gapless quantum spin liquid which has a Fermi surface of spin-$\frac{1}{2}$ neutral quasiparticles, the spinons, while the charge excitations are fully gapped. Consequently, there is a single-particle gap in the electron spectral function even though there are gapless spin-carrying excitations. This type of spin-charge separation where only the charge localizes can be favored in systems (such as the organics) where frustration and charge fluctuations suppress magnetic ordering.

The MIT we consider was studied at the mean-field level in Ref. 2. A subsequent analysis[5] of the quantum fluctuations provided evidence that the second-order nature can survive the (inevitable) inclusion of many-body effects. A rich set of properties associated with the quantum critical point (QCP) was uncovered, many not present at the mean-field level. For example, it was found that quantum fluctuations lead to a divergence of the effective FL mass as one approaches the MIT. This gives rise to a divergence of the specific heat capacity coefficient $\gamma = C/T$. A key insight was the realization that the quantum critical state at the edge between the FL and SL is actually a non-FL (nFL) metal where the Landau quasiparticle is destroyed but the concept of a sharp Fermi surface persists. This was dubbed a "critical Fermi surface."[4,5] One prediction of this theory was that the zero-temperature resistivity jumps by a finite amount as one goes from the FL to the quantum critical state, where the value of the jump was predicted to be universal, $R\hbar/e^2$, R being a dimensionless number associated with the QCP. This resistivity jump is illustrated in Fig. 1.

The main purpose of this work is to provide a controlled calculation of the value of this jump and, more generally, analyze the behavior of the electric resistivity in response to changes in pressure (modifying the metallic bandwidth) and/or temperature in the vicinity of the QCP. The resulting resistivity can be compared with experiments, where the bandwidth can be changed by applying mechanical or chemical pressure. The predictions we make, viz., sharp resistivity variation on the order of $10h/e^2 \sim 100$ kΩ, quantum critical collapse of pressure and temperature dependencies, thermal conductivity

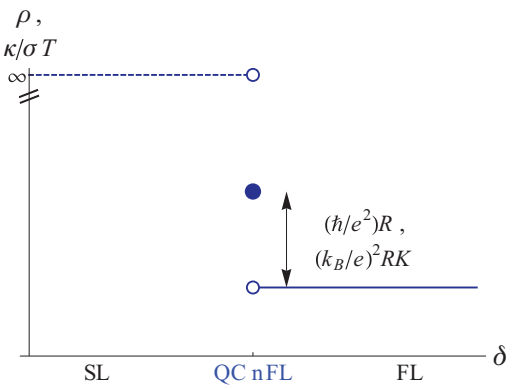

FIG. 1. (Color online) Jump of the universal resistivity ρ and Lorentz number $\kappa/\sigma T$ at $T = 0$ as a function of δ, which is proportional to ratio of the bandwidth to the Hubbard repulsion [Eq. (1)]. The latter jump signals a violation of the Wiedemann-Franz law by the critical Fermi-surface state. κ is the thermal conductivity; R, K are universal constants associated with the Mott QCP. In particular, they strongly depend on the emergent gauge boson associated with the electron fractionalization. The resistivity becomes infinite in the SL, and as a consequence so does the Lorentz number.

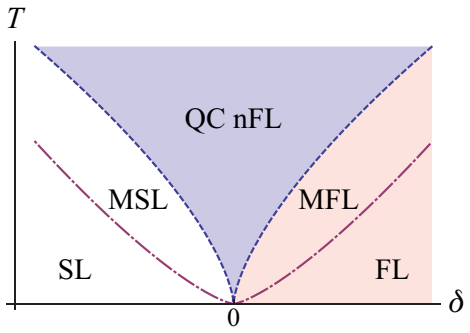

FIG. 2. (Color online) The phase diagram of the quantum critical Mott transition. δ tunes the ratio of onsite repulsion to the bandwidth away from its critical value, and can be put in correspondence with $P - P_c$, the deviation from the QC pressure P_c. The dark shaded (blue) region is the quantum critical region, where the Landau quasiparticle is destroyed but a "critical Fermi surface" nonetheless exists. It separates the spin liquid (SL) and the Fermi liquid (FL). The intermediate-T states (with prefix "M"), the marginal SL and FL, differ from the low-temperature ones by the fact that the spinons and gauge bosons still behave as in the QC region.

jump, and violation of Wiedemann-Franz law, provide distinct signatures of the fractionalization at the MIT and of the critical Fermi-surface state intervening between the FL and SL.

A crucial ingredient of the theory is that, at zero temperature, the emergent gauge fluctuations associated with the fractionalization decouple from the quantum critical charge fluctuations. Despite this, the gauge fluctuations are expected to play a crucial role for nonzero-temperature transport properties. A similar phenomenon happens in the Kondo breakdown model studied in Ref. 20. An important difference with the Kondo breakdown scenario is that the charge fluctuations near the Mott transition studied in this paper are described by an interacting field theory at low energies. Irrespective of this difference, the same conclusion holds: the gauge fluctuations become important for low-frequency transport at nonzero temperature. We show this explicitly by calculating the effects of these gauge fluctuations on the transport. In particular, the precise value of the universal resistivity jump in the limit that the frequency of the applied electric field goes to zero faster than temperature is strongly affected by the gauge fluctuations. In contrast, in the opposite order of limits the universal resistivity jump is unaffected by the gauge field. We further predict a universal jump of the thermal conductivity across the Mott transition, which derives from the breaking of low-energy conformal invariance by the gauge field, and leads to a violation of the Wiedemann-Franz law by the critical Fermi surface.

The paper is organized as follows. In Sec. II, we summarize our main findings; Sec. III introduces the slave-rotor description for the Hubbard model. In Sec. IV, we formulate the transport via a quantum Boltzmann equation for the critical charge fluctuations, the rotors, and present its solution at criticality. Section V extends the resistivity calculation to the entire QC region. In Sec. VI, we discuss the behavior of the resistivity at large temperatures and frequencies. Signatures relating to thermal transport are discussed in Sec. VII. The Appendixes give further details regarding the critical rotors, with a focus on their transport properties in the absence of the emergent gauge field, i.e., in the pure $O(N)$ nonlinear sigma model (NLσM) for $N \geqslant 2$.

II. MAIN RESULTS

In this section, we summarize our main results. We first need to briefly describe the finite-temperature phase diagram obtained in Ref. 5, which is reproduced in Fig. 2. The parameter δ tunes the ratio of the electronic bandwidth to the onsite repulsion away from its critical value, and can be put in correspondence with $P - P_c$, the deviation from the quantum critical pressure P_c:

$$\delta \propto t/U - (t/U)_c \sim P - P_c \,. \tag{1}$$

At $T > 0$, the metal-insulator transition becomes a crossover due to the presence of the emergent gauge boson. We distinguish three main phases in Fig. 2: the spin liquid (in white in the figure), the Fermi liquid (pink/light shading), and the quantum critical state bridging the two (blue/dark shading). The latter state is a non-FL where the Landau quasiparticle has been destroyed, yet a sharp Fermi surface persists: an instance of a "critical Fermi surface." In exiting the QC region, one enters two intermediate phases: a marginal spinon liquid (MSL) or a marginal Fermi liquid (MFL). These are similar to their low-temperature counterparts, the SL and FL, except that the spinons and gauge bosons still behave as in the QC region. As these correspond to fluctuations in the spin degrees of freedom, the two crossovers may be interpreted as corresponding to spin and charge degrees of freedom exiting criticality at parametrically different temperatures. At sufficiently low temperature they cross over to the usual SL and FL states. The behavior of the electric resistivity as one tunes across the phase diagram is illustrated in Fig. 3. Figures 3(a) and 3(c) correspond to the T-dependent behavior at fixed δ (i.e., pressure), and vice versa for 3(b) and 3(d). The important crossovers for low-temperature transport are

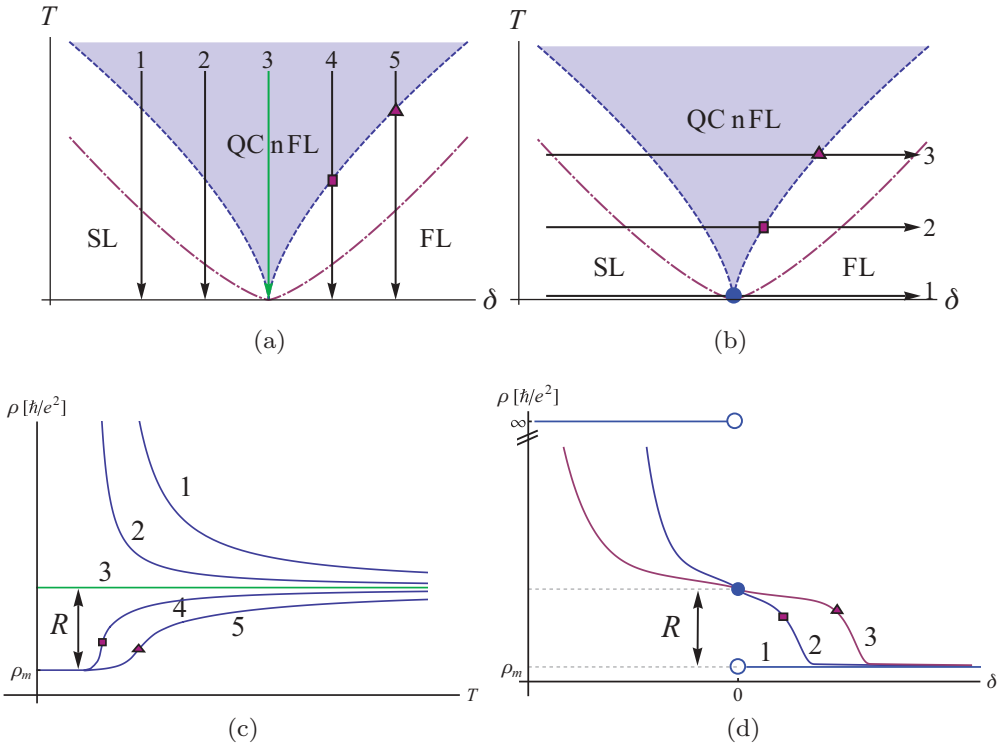

FIG. 3. (Color online) Sketch of low-temperature behavior of the resistivity near the quantum critical (QC) Mott transition. Panel (c) shows the resistivity vs T for different values of the onsite repulsion over the bandwidth (tuned by δ), with the corresponding cuts shown in the phase diagram in (a). Panel (d) shows the resistivity vs δ at different temperatures, with the corresponding cuts shown in the phase diagram in (b). In (c) and (d), the markers correspond to the location of the resistivity jump upon entering the QC state from the FL. The value of the jump is universal: $R\hbar/e^2$. Our calculations yield $R = 49.8$, which translates to a jump of $\sim 8h/e^2$.

the boundaries of the QC region: there, the charge degree of freedom either localizes (SL) or condenses (FL). At the former crossover the resistivity becomes thermally activated, $\sim e^{\Delta_+/T}$, because of the finite Mott charge gap Δ_+. This can be seen in curves 1 and 2 in Fig. 3(c). At the crossover to the FL, it abruptly drops to its residual metallic value ρ_m [curves 4 and 5 in Fig. 3(c)]. The regime of interest for transport corresponds to the QC non-FL, where the resistivity relative to its residual value in the metal ρ_m is purely universal: $\rho - \rho_m \approx (\hbar/e^2)R$, where R is a universal dimensionless constant. Our controlled calculation of R in a large-N approximation gives the estimate $R = 49.8$. R sets the size of the jump shown in Fig. 1, which is reproduced in Fig. 3(d), curve 1. At finite temperature, this jump becomes a steep increase, as shown in curves 2 and 3 of Fig. 3(d). We emphasize that the low-temperature resistivity above the QCP, $\delta = 0$, is T independent and takes the value $\rho = \rho_m + (\hbar/e^2)R$.

The diverse behavior shown in Fig. 3 can be obtained from a single-variable function. Indeed, the temperature- and pressure-dependent resistivity (relative to its constant residual value in the FL) can be collapsed by a universal scaling function G associated with the Mott QCP:

$$\rho - \rho_m = \frac{\hbar}{e^2} G\left(\frac{\delta^{z\nu}}{T}\right), \tag{2}$$

where the dynamical and correlation length exponents correspond to those of the three-dimensional (3D) XY universality class: $z = 1$ and $\nu \approx 0.672$. Indeed, the critical charge degrees of freedom can be effectively described by a Bose-Hubbard model at half-filling near its insulator-superfluid transition, which belongs to that universality class. We show that although the spin fluctuations encoded in the emergent gauge field associated with the electron fractionalization do not alter these exponents, they have strong effects on the scaling function, and thus on the value of the universal jump $(\hbar/e^2)R$.

We predict that thermal transport also shows signatures of the critical Fermi surface. In particular, the thermal conductivity divided by temperature κ/T has a universal jump at criticality, by an amount $(k_B^2/\hbar)K$, where K is a dimensionless number just like R. As we explain in Sec. VII, the emergent gauge fluctuations play an important role by breaking the conformal invariance present in their absence, thus reducing κ/T from a formally infinite value to a finite, universal one. Finally, combining the electric resistivity and thermal conductivity jumps, we predict that the QC non-FL violates the Wiedemann-Franz law by a universal amount: the Lorentz number differs from its usual value in the FL by $(k_B/e)^2 RK$, as shown in Fig. 1.

III. MOTT TRANSITION IN THE HUBBARD MODEL: A SLAVE-ROTOR FORMULATION

To set the stage, we briefly review the description of the insulating quantum spin liquid with a spinon Fermi surface,[3] and the continuous bandwidth-tuned Mott transition[5] to it from

a Fermi liquid. We consider a single-band Hubbard model at half-filling on a two-dimensional (2D) nonbipartite lattice (for, e.g., triangular):

$$H = -t \sum_{\langle rr' \rangle} (c^\dagger_{\sigma r} c_{\sigma r'} + \text{H.c.}) + U \sum_r (n_r - 1)^2, \qquad (3)$$

where $c_{\sigma r}$ annihilates an electron with spin σ at site r, and $n_r = c^\dagger_{\sigma r} c_{\sigma r}$. In the small-$U/t$ limit, the ground state is a Fermi-liquid metal, while in the opposite limit a Mott insulator results. The interplay of frustration and strong charge fluctuations can lead to a quantum spin-liquid ground state instead of a conventional antiferromagnetic Mott insulator. We shall focus on the transition to such a state.

The slave-rotor construction[2] is tailor made to describe the spin-charge separation that occurs as the charge localizes when the electronic repulsion becomes sufficiently large, yet weak enough for the spins to remain disordered, even at $T = 0$. At the level of the microscopic Hubbard model [Eq. (3)], the slave-rotor construction is a change of variables to degrees of freedom better suited to describe the SL, in which the electron is fractionalized into spin- and charge-carrying "partons":

$$c_{r\sigma} = \psi_{\sigma r} b_r \,. \qquad (4)$$

The fermionic spinons $\psi_{\sigma r}$ carry the spin, while the bosonic rotors $b_r = e^{-i\theta_r}$ the charge of the original electron. The projection from the enlarged Hilbert space to the physical one is obtained from the operator identity relating the rotor charge or "angular momentum" l_b to the fermion number, n_f: $l_b = 1 - n_f$, which is enforced at each site, where $n_f = n$ is the actual electronic occupation number (because $|b| = 1$). By virtue of Pauli exclusion, the charge relative to half-filling at each site can only be -1 (double occupancy), $+1$ (hole), and 0 (single occupancy). Hence, the positive (holon) and negative (doublon) electric charge excitations encoded in the rotors relate to the holes and doubly occupied sites of the half-filled Hubbard model (see Fig. 4). Moreover, since the system is at half-filling, there is a low-energy particle-hole symmetry between these positive and negative charge excitations.

In the long-wavelength limit, a U(1) gauge structure emerges.[3] The temporal component of the gauge field results from the above constraint necessary to recover the physical Hilbert space, while the spatial components derive from the fluctuations of spinon bilinears about their saddle-point configuration. After coarse graining, the low-energy effective action for the Hubbard model in terms of the fractionalized degrees of freedom can be written as

$$S = S_{b,a} + S_{f,a} + S_a \,, \qquad (5)$$

$$S_{b,a} = \frac{1}{2g} \int_x (|(\partial_\nu - i a_\nu) b|^2 + i\lambda(|b|^2 - 1)) \,, \qquad (6)$$

$$S_{f,a} = \int_x \bar{\psi}_\sigma \left(\partial_\tau - \mu - i a_0 + \frac{(\boldsymbol{\nabla} - i \boldsymbol{a})^2}{2 m_f} \right) \psi_\sigma \,, \qquad (7)$$

$$S_a = \frac{1}{e_0^2} \int_x (\epsilon^{\nu\gamma\beta} \partial_\gamma a_\beta)^2 . \qquad (8)$$

We work in units where the rotor velocity c is set to one, unless otherwise specified. The complex boson field b is constrained to lie on the unit circle via the Lagrange multiplier field λ. The indices ν, γ, β run over imaginary time and the two spatial dimensions; μ is the electronic chemical potential. We have used the shorthand $\int_x = \int_0^{1/T} d\tau \int d^2x$. The gauge fluctuations have a Maxwellian action resulting from the elimination of high-energy fluctuations; e_0 is the corresponding bare gauge charge. The parameter that tunes the Mott transition of the rotors (and hence of the whole electronic liquid) is $g \propto U/t$, where U is the Hubbard repulsion from the original electronic Hamiltonian, while t is proportional to the electronic bandwidth. To make the action dimensionless, the parameter g carries the dimension of length, as given by a real-space cutoff scale. We can relate it to the parameter δ introduced in Eq. (1) via $\delta = g^{-1} - g_c^{-1} \propto t/U - (t/U)_c$. For small coupling $g < g_c$, the rotors spontaneously condense, corresponding to the metallic phase of the original Hamiltonian, while in the opposite limit $g > g_c$, the rotor field is disordered, leaving the system in a SL ground state. In the condensed or ordered phase, one key feature that needs to be emphasized is the gapping out of a spurious "gapless zero sound mode" found in the decoupled treatment,[2] where it arises as a Goldstone boson of the spontaneously broken $O(2)$ symmetry of the charged rotors in the FL. In fact, this mode acquires a gap when the inescapable gauge fluctuations about the saddle point are included. The Goldstone boson combines with the emergent transverse gauge boson via the Anderson-Higgs mechanism, which leaves both excitations with a gap.

The emergence of a relativistic action for the rotors, which have a dynamical exponent $z = 1$, is a consequence of the emergent low-energy particle-hole symmetry of the Hubbard model at half-filling noted above. This low-energy symmetry will be important when we examine the effect of the gauge field on the critical rotors. It will lead to a strong suppression of the dynamical gauge fluctuations in the charge (rotor) sector.

The field theory above is strongly interacting. Indeed, in two dimensions the rotor NLσM considered separately flows to a strong-coupling fixed point where even the b-field quasiparticles are ill defined. The spinons and gauge fluctuations do not alter this. One perturbative approach to the problem extends the field theory to include a large number of flavors of the matter fields: when that number is very large, we have weakly interacting quasiparticles, at least in the boson

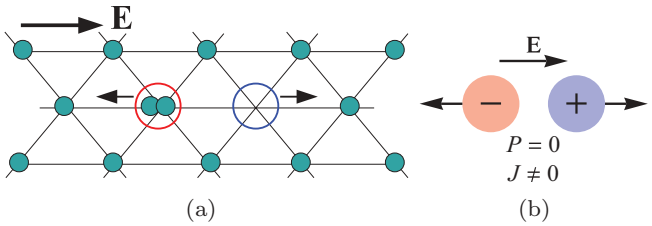

FIG. 4. (Color online) Charge excitations near the Mott transition. (a) Triangular lattice at half-filling; the small shaded disks represent electrons. The double-occupied (empty) sites are identified by a red/left (blue/right) circle. These are encoded in the charge rotor excitations, the holons and doublons, respectively. Under an applied electric field, they will move in opposite directions. (b) By virtue of the emergent particle-hole symmetry between doublons and holons, it is possible to have a state with zero momentum P but finite current J. This allows interactions to dissipate current while conserving momentum.

sector. We will use this extension, which we now describe in more detail, to bring the calculation under control.

A. Low-energy theory and large-N extension

We consider the slave-rotor field theory extended to have a large number of rotor and spinon flavors, allowing for a systematic study of transport.[21] The number of copies of the complex rotor is taken to be $N/2$, yielding an even number N of real scalar fields. The case of physical interest has $N = 2$. In this large-N extension, the effective actions of the rotors and spinons read as

$$S_{b,a} = \frac{N}{2g}\int_x (|(\partial_\nu - i a_\nu) b_\alpha|^2 + i\lambda(|b_\alpha|^2 - 1)), \quad (9)$$

$$S_{f,a} = \int_x \bar{\psi}_\sigma \left(\partial_\tau - \mu - i a_0 + \frac{(\boldsymbol{\nabla} - i\boldsymbol{a})^2}{2m_f}\right)\psi_\sigma, \quad (10)$$

where each b_α is a complex scalar, and α runs from 1 to $N/2$, while there are N copies of spinons, $\sigma = 1,\ldots,N$. Repeated indices are summed over, for example, $|b_\alpha|^2 = \bar{b}_\alpha b_\alpha = \sum_\alpha |b_\alpha|^2$. λ is the Lagrange multiplier field enforcing the constraint that the $O(N)$ real field be unimodular. The coupling g has been rescaled $g \to g/N$. Note that the gauge field reduces the rotor global symmetry from $O(N)$ to $U(N/2)$. In the $N \to \infty$ limit, the fluctuations of the λ and gauge bosons are unimportant. Formally integrating out the rotors yields the following form for the partition function[21] $\mathcal{Z} = \int \mathcal{D}\lambda e^{-S_{\rm eff}[\lambda]}$, with

$$S_{\rm eff}[\lambda] = \frac{N}{2}\left[\mathrm{tr}\ln(-\partial^2 + i\lambda) - \frac{i}{g}\int_x \lambda\right]. \quad (11)$$

The overall factor of N plays the role of $1/\hbar$ so that in the large-N limit, the quantum fluctuations are suppressed and we only need to consider the classical equation of motion[21]

$$\int_q \frac{1}{q^2 + m^2} = \frac{1}{g}, \quad (12)$$

where $\int_q = T\sum_{\omega_n}\int d^d q/(2\pi)^d$ and the mass squared $m^2 = i\lambda_0 \in R$ corresponds to the saddle-point value of the uniform component of λ, λ_0. This mean-field value of λ plays the role of the mass for the rotors in their insulating phase at large g. It can be alternatively seen as the inverse correlation length $\xi \sim 1/m$. At sufficiently small g, Eq. (12) has no solution, and a different approach must be used to describe the condensation. In the following, we shall focus mainly on the quantum critical regime as well as on the insulating phase. The solution of the saddle-point equation (12) in the large-N limit and at finite temperature directly above the quantum critical point $g = g_c$ yields $m = \Theta T$, where $\Theta = 2\ln(\frac{1+\sqrt{5}}{2}) \approx 0.96$, twice the logarithm of the golden ratio.[22] The mass vanishes linearly as $T \to 0$, i.e., the correlation length of the charged rotors diverges upon approaching the QCP: $\xi \sim 1/T$. The full dependence of m on g and T at $N = \infty$ is given in Sec. V.

Corrections at order $1/N$ to the $N = \infty$ saddle point correspond to interactions mediated by the λ and a bosons, which develop dynamics when N is finite. The rotor action, including the effective mass corresponding to the saddle-point value of the λ boson, now reads as

$$S_{b,a} = \frac{1}{2g}\int_x [|(\partial_\nu - i a_\nu) b_\alpha|^2 + m^2|b_\alpha|^2 + i\lambda|b_\alpha|^2]. \quad (13)$$

We are using the Coulomb or transverse gauge so that it is understood that we only include configurations where $\boldsymbol{\nabla}\cdot\boldsymbol{a} = 0$. The transverse and temporal component of a_μ are decoupled in this gauge. Further, we can omit the latter in the low-energy limit because it is screened by the spinon Fermi surface. The transverse part of the gauge field remains gapless because the currents remain unscreened, as opposed to the charge. In the remainder, we shall use a to represent the transverse component. The $1/N$ corrections to the saddle point will generate $\mathcal{O}(1/N)$ propagators for both the gauge and λ bosons, which acquire the following effective action:

$$\frac{1}{2}\int_q \left[|a(q)|^2\frac{N}{2}\left(\Pi^{\rm j}_f + \Pi^{\rm j}_b\right) + |\lambda(q)|^2\frac{N}{2}\Pi_b\right], \quad (14)$$

where the finite-temperature, imaginary-time polarization functions read as

$$\Pi_b(i\nu_l, q) = T\sum_n \int \frac{d^2\boldsymbol{p}}{(2\pi)^2}\frac{1}{(\omega_n + \nu_l)^2 + \epsilon^2_{p+q}}\frac{1}{\omega_n^2 + \epsilon_p^2}, \quad (15)$$

$$\Pi^{\rm j}_b(i\nu_l, q) = -T\sum_n \int \frac{d^2\boldsymbol{p}}{(2\pi)^2}\frac{(2\hat{q}\times\boldsymbol{p})^2}{(\omega_n + \nu_l)^2 + \epsilon^2_{p+q}}\frac{1}{\omega_n^2 + \epsilon_p^2}, \quad (16)$$

where the superscript "j" identifies the current-current correlator; we have defined the rotor dispersion relation $\epsilon_p = \sqrt{p^2 + m^2}$. Details about the computation of $\Pi_b, \Pi^{\rm j}_b$ can be found in Appendixes A and C, respectively. $\Pi^{\rm j}_b$ is discussed in the next section. The spinon Fermi surface contributes

$$\Pi^{\rm j}_f = \mu\left(c_1\frac{|\omega_n|}{v_F k} + c_2\frac{k^2}{k_F^2}\right), \quad |\omega_n| < v_F k \quad (17)$$

where the c_i are real numbers, while k_F, v_F are the Fermi momentum and velocity, respectively. As we work in units where the velocity of the rotors is set to 1, we need to keep v_F explicitly. Because of the term $|\omega_n|/v_F k$ in the fermionic polarizability, the gauge fluctuations are Landau damped.

1. Role of gauge fluctuations

We now examine the role of the gauge fluctuations. The Landau damped dynamics due to the Fermi surface dominate those induced by the rotor polarization function $\Pi^{\rm j}_b$, and we can evaluate the latter in the static limit.[5] Note that $\Pi^{\rm j}_b$, just as Π_b, depends on the temperature and g via the mass of the rotors m. For $g = g_c$, as shown in Appendix C, we get

$$\Pi^{\rm j}_b(0,q) = \begin{cases} \gamma_2\frac{q^2}{T} & \text{if} \quad q \ll T, \\ \sigma_b^\infty q & \text{if} \quad q \gg T, \end{cases} \quad (18)$$

where $\gamma_2 \approx 0.031$ is a dimensionless constant, while $\sigma_b^\infty \approx 0.063$ is the rotor conductivity in units of $e^2/\hbar$ in the large-frequency ($T \to 0$) limit $\omega/T \gg 1$. As discussed in Secs. IV A and VI A, it differs from the dc conductivity we are seeking and can be obtained from a simple $T = 0$ analysis. The q^2 behavior at $q \ll T$ results from including the mass of

the rotors $m = \Theta T$ when computing the current polarization function. It has the behavior expected from massive modes since for $q \ll T$, the fluctuations exceed the correlation length $1/m \sim 1/T$ and must be gapped. The important term for the low-temperature behavior is the linear q contribution. This nonanalytic dependence arises because of the gaplessness of the critical rotors and gives the gauge field a $z_a = 2$ dynamical exponent, making it less singular than deep in the SL where the rotors are gapped and the gauge bosons have $z_a = 3$. Indeed, the $z_a = 2$ damped gauge fluctuations give the spinons a self-energy $\sim \frac{1}{N} i\omega \ln(\mu/|\omega|)$, which is weaker than in the usual SL, where we have $\frac{1}{N} i|\omega|^{2/3}$. Thus, at criticality, as well as in the MFL and MSL phases, the spinons form a marginal Fermi liquid, leading to the usual logarithmic corrections. We emphasize that we do not need to worry about possible subtleties with the breakdown of the naive large-N expansion for a Fermi surface coupled to a gapless boson.[23] Indeed, we are mainly concerned with the quantum critical region, where, as stated above, the fermions only acquire logarithmic corrections due to gauge fluctuations. Such a marginal Fermi liquid of spinons can be controlled by a simple perturbative renormalization group (RG) approach.[24,25] In contrast, deep in the SL, one might need to take the limit of small $z_a - 2$ simultaneously with $1/N \to 0$ to make the expansion controlled.[25] Further, the main transport properties will derive from the rotor sector for which the large N works reliably. The spinons affect the rotors only via the damping of the gauge bosons, which we believe is a robust feature, independent of the expansion scheme.

Regarding the rotor or charge sector, it was shown[5] that the gauge fluctuations do not alter the nature of the rotor excitations, i.e., the rotor self-energy is subleading compared to the bare dynamics. Insofar as the thermodynamic critical properties of the charge sector are concerned, they belong to the 3D XY universality class, unaffected by the gauge bosons or spinons. The importance of the damping at quenching the gauge fluctuations can be heuristically understood by examining the dominant rotor fluctuations, which have $\omega \sim q$ ($z = 1$). Substituting this dispersion relation into the Landau damping term we get $\mu|\omega|/q \sim \mu$. Thus, the dominant rotor fluctuations see the gauge bosons as screened. Such an effect was also identified in Ref. 26, in the context of a quantum critical transition between a Néel-ordered Fermi-pocket metal to a non-FL algebraic charge liquid, called a "doublon metal." This suppression mechanism of the gauge field due to a Fermi surface was referred to as a "fermionic Higgs effect."

In the next section, we shall show that although the gauge fluctuations are not effective at influencing the thermodynamic critical properties in the charge sector, they can have strong effects on nonzero-temperature transport, down to arbitrarily low temperatures.

IV. CRITICAL TRANSPORT NEAR THE MOTT TRANSITION

In a slave-particle theory such as the one under consideration, many observables can be determined from the separate responses of the partons. These relations generally go under the name of Ioffe-Larkin composition rules. For example, the one for the resistivity reads as[27]

$$\rho = \rho_b + \rho_f \,, \tag{19}$$

where $\rho_{b,f}$ is the resistivity of the spinons and rotors, respectively. The resistivities "add in series" because of the constraint relating the spinons and rotors to recover the original Hamiltonian/Hilbert space: the electric field induces a motion of the electrically charged rotors, forcing spinons to flow as well. Alternatively, we can say that the external electric field induces an internal one. It follows that the parton with the highest resistivity governs the entire electric response. Near the Mott transition, the rotors have the most singular response as they undergo a quantum phase transition, while the spinons form a Fermi surface throughout. We thus anticipate that the strong variation of ρ_b across the transition will give the entire resistivity its key dependence.

Let us first discuss the $T = 0$ and clean limit, in which case the spinon Fermi surface has vanishing resistivity throughout. The rotors also have vanishing resistivity in their condensed phase, such that the FL has $\rho = \rho_b + \rho_f = 0 + 0 = 0$ as expected. On the Mott side, the rotors are gapped hence the whole system has infinite resistivity: $\rho_b = \infty = \rho$. The interesting feature happens directly at criticality, where although we still have $\rho_f = 0$, the rotors have a finite universal resistivity induced purely by interactions[22,28] $\rho_b = R\hbar/e^2$. It is possible for systems with particle-hole symmetry or equivalently emergent relativistic invariance to have a finite resistivity in the absence of disorder or umklapp scattering. For such systems, the momentum and electric current operators need not be proportional, allowing interactions to dissipate the latter while preserving the former. More physically, these systems have independent and symmetry-related positive and negative charge excitations that flow in opposite directions under an applied electric field, yielding a state with a finite current but with zero momentum. This is schematically illustrated in Fig. 4. The finite, interaction-driven rotor resistivity at criticality leads to a discrete jump at $T = 0$, as illustrated in Fig. 1.

This scenario naturally extends to finite but low temperatures: the fermions still contribute only a constant ρ_f, which is zero for a clean system, or finite in the presence of weak disorder. Instead of discontinuously jumping, the rotor resistivity increases rapidly upon entering the quantum critical region, where it slowly increases until the growth becomes exponential at the crossover to the spin liquid, as is shown in Fig. 3(d). We shall thus focus on the resistivity of the rotors ρ_b for which we perform a $1/N$ expansion. In the simplest limit, $N = \infty$, the rotors are free because they decouple from the λ and gauge bosons. The dc resistivity thus vanishes in the absence of scattering, $\rho_b = 0$. At order $1/N$, the rotors begin colliding with the constraint field λ and the emergent gauge boson, leading to a finite resistivity. For sufficiently large N, the system has well-defined quasiparticles, the transport properties of which can be unambiguously studied by a quantum kinetic (or Boltzmann) equation, to which we now turn.

A. Quantum Boltzmann equation for critical charge fluctuations

We formulate the quantum Boltzmann equation (QBE) for the distribution functions of the rotor excitations in the presence of an oscillating electric field $\boldsymbol{E}(t)$ with driving frequency ω. This frequency plays an important role as it introduces an energy scale that divides the critical frequency-dependent

resistivity into two regimes: $\omega < T$ and $\omega > T$. Indeed, the frequency ω must be compared with the dominant scale for the rotors in the quantum critical regime, which is the temperature. As was established in seminal work by Damle and Sachdev,[22] the limits $\omega \to 0$ and $T \to 0$ do not generally commute for the response functions of critical systems. For example, the $T = 0$ dc resistivity is obtained by first taking $\omega/T \to 0$, then $T \to 0$, so that one must necessarily perform a finite-temperature analysis to obtain the correct dc response. A $T = 0$ calculation, which is equivalent to taking $T \to 0$ first, yields the response in the $\omega/T \to \infty$ limit, which generically differs from the dc behavior. This noncommutativity of the $\omega \to 0$ and $T \to 0$ limits can be explained on physical grounds: The small-frequency resistivity ($\omega < T$) is dominated by the incoherent scattering of thermally excited critical fluctuations; it corresponds to the hydrodynamic limit. In contrast, the large-frequency resistivity ($\omega > T$) arises from the coherent motion of field-generated excitations; it is mainly collisionless. The dichotomy is even more striking in our case due to the presence of the gauge bosons: We shall show that although the gauge fluctuations do not affect the transport in the large-ω/T limit, they actually dominate the dc resistivity!

We assign the electric charge to a single rotor flavor b_1, which couples to the oscillating electric field $\boldsymbol{E}(t)$. The standard mode expansion for the electrically charged rotor operator reads as

$$b_1(x) = \int_{\boldsymbol{k}} \alpha_+(t,\boldsymbol{k})e^{i\boldsymbol{k}\cdot\boldsymbol{x}} + \alpha_-^\dagger(t,\boldsymbol{k})e^{-i\boldsymbol{k}\cdot\boldsymbol{x}}, \tag{20}$$

where we have defined $\alpha_\pm/\alpha_\pm^\dagger$ as the annihilation/creation operators for holons (+) and doublons (−), i.e., the positive and negative electric charge excitations. The expectation value of the current can be decomposed into two pieces: $\boldsymbol{J}(t) = \boldsymbol{J}_I(t) + \boldsymbol{J}_{II}(t)$, where

$$\boldsymbol{J}_I(t) = \int_{\boldsymbol{k}} \sum_{s=\pm} s\frac{\boldsymbol{k}}{\epsilon_k}\langle\alpha_s^\dagger(t,\boldsymbol{k})\alpha_s(t,\boldsymbol{k})\rangle \tag{21}$$

$$= \int_{\boldsymbol{k}} \sum_{s=\pm} s\frac{\boldsymbol{k}}{\epsilon_k} f_s(t,\boldsymbol{k}), \tag{22}$$

$$\boldsymbol{J}_{II}(t) = \int_{\boldsymbol{k}} \frac{\boldsymbol{k}}{2\epsilon_k}\langle\alpha_+^\dagger(t,-\boldsymbol{k})\alpha_+^\dagger(t,\boldsymbol{k}) - \alpha_-^\dagger(t,-\boldsymbol{k})\alpha_-^\dagger(t,\boldsymbol{k}) - 2\alpha_+^\dagger(t,-\boldsymbol{k})\alpha_-^\dagger(t,\boldsymbol{k})\rangle + \text{H.c.} \tag{23}$$

We have defined the distribution functions of positive and negative charge excitations: $f_s = \langle\alpha_s^\dagger(t,\boldsymbol{k})\alpha_s(t,\boldsymbol{k})\rangle$, $s = \pm$; $\epsilon_k = \sqrt{m^2 + k^2}$ is the rotor dispersion. From Eq. (23), it should be apparent that as $\boldsymbol{J}_{II}$ involves pair production, it will only contribute when the driving frequency is above the pair-production threshold $\omega > 2m$, where $m \sim T$ in the QC region. We shall concern ourselves with the determination of $\boldsymbol{J}_I$, i.e., $f_s(t,\boldsymbol{k})$, which governs the transport in the small-frequency limit. The asymptotic high-frequency resistivity in the limit $\omega \gg T$ can be obtained from a $T = 0$ calculation and we leave its analysis to Sec. VI A.

The QBE for the distribution function of holon (doublon) rotor excitations f_s with $s = \pm$, respectively, reads as

$$(\partial_t + s\boldsymbol{E}\cdot\partial_{\boldsymbol{k}})f_s(\boldsymbol{k},t) = \frac{1}{N}(I_\lambda[f_\pm] + I_a[f_\pm]) \tag{24}$$

$$\begin{aligned}= \frac{2}{N}\int_0^\infty \frac{d\Omega}{\pi}\int\frac{d^2q}{(2\pi)^2}\left[\text{Im}\left(\frac{1}{\Pi_b(\Omega,q)}\right) + (2\boldsymbol{k}\times\hat{\boldsymbol{q}})^2\,\text{Im}D(\Omega,q)\right]\Bigg\{&\frac{(2\pi)\delta(\epsilon_k - \epsilon_{k+q} - \Omega)}{4\epsilon_k\epsilon_{k+q}}[f_s(\boldsymbol{k},t)[1 + f_s(\boldsymbol{k}+\boldsymbol{q},t)] \\ \times[1 + n(\Omega)] - f_s(\boldsymbol{k}+\boldsymbol{q},t)[1 + f_s(\boldsymbol{k},t)]n(\Omega)] + &\frac{(2\pi)\delta(\epsilon_k - \epsilon_{k+q} + \Omega)}{4\epsilon_k\epsilon_{k+q}}[f_s(\boldsymbol{k},t)[1 + f_s(\boldsymbol{k}+\boldsymbol{q},t)]n(\Omega) \\ - f_s(\boldsymbol{k}+\boldsymbol{q},t)[1 + f_s(\boldsymbol{k},t)][1 + n(\Omega)]] + &\frac{(2\pi)\delta(\epsilon_k + \epsilon_{-k+q} - \Omega)}{4\epsilon_k\epsilon_{-k+q}}[f_s(\boldsymbol{k},t)f_{-s}(-\boldsymbol{k}+\boldsymbol{q},t)[1 + n(\Omega)] \\ - [1 + f_s(\boldsymbol{k},t)][1 + f_{-s}(-\boldsymbol{k}+\boldsymbol{q},t)]n(\Omega)]\Bigg\}.\end{aligned} \tag{25}$$

We have absorbed the magnitude of the rotor charge into $\boldsymbol{E}$. The right-hand side of the QBE, the collision term, can be obtained for instance by invoking Fermi's golden rule.[21,29] The first two δ functions enforce energy conservation for absorption and emission of λ and gauge bosons by the rotors, while the last one corresponds to pair creation/annihilation of holon-doublon pairs.

The propagators of the λ and gauge bosons $2/N\Pi_b$ and $2D/N = 2/N(\Pi_j^{\text{j}} + \Pi_b^{\text{j}})$, respectively, enter into the QBE via their spectral functions which dictate the density of states the rotor excitations can scatter into. They are evaluated in equilibrium. This is justified in the large-N limit since the external field couples to a single rotor flavor such that the associated nonequilibrium corrections to the polarization functions sublead in $1/N$. In other words, the drag of the λ and gauge fields by the electric field, an analog of "phonon drag," is negligible in the large-N regime. The rotor flavors that do not directly couple to the electric field $b_{\alpha>1}$ play the role of an effective bath at equilibrium, from which the constraint field acquires its dynamics.

The scattering terms on the right-hand side of Eq. (24) all scale like $1/N$ because the gauge and λ bosons have propagators of that order. As $N \to \infty$, the scattering terms vanish and the rotors become free, displaying a sharp Drude peak in the real part of the small-frequency conductivity: $\sigma_b \propto \delta(\omega)$, $\omega < T$. As we shall see, the finite $1/N$ effects will cure this singularity, yielding a finite dc conductivity.

We now proceed to the solution of the rotor QBE [Eq. (24)] by first expanding the distribution function to linear order in $\boldsymbol{E}$,

$$f_s(\boldsymbol{k},\omega) = n(\epsilon_k)2\pi\delta(\omega) + s\boldsymbol{E}\cdot\boldsymbol{k}\varphi(k,\omega)\,, \tag{26}$$

where we have Fourier transformed from time to frequency. The deviation function $\varphi(k,\omega)$ only depends on the magnitude of $\boldsymbol{k}$ since $\boldsymbol{E}\cdot\boldsymbol{k}$ fully encodes the rotational symmetry breaking in the presence of the external electric field. The unknown function φ parametrizes departures from the equilibrium Bose-Einstein distribution $n(\epsilon_k)$, with $\epsilon_k^2 = m^2 + k^2$. The result of the linearization of the collision term due to the λ bosons can be found in Appendix A; we can not make significant simplifications there. Indeed, we need to perform a careful numerical evaluation of the retarded polarization function $\Pi_b(\Omega,q)$ for all frequencies and momenta. On the other hand, we can significantly simplify the scattering term due to gauge bosons. As mentioned above, dynamical gauge fluctuations are suppressed in the rotor sector at $T=0$. Although a static ($\Omega=0$) gauge mode $a(0,\boldsymbol{q})$ escapes the Landau damping, at $T=0$ it constitutes a set of measure zero in the continuum of excitations and is thus unimportant. At finite T, the static $\Omega_n = 0$ Matsubara frequency is well separated from the others and thus provides a viable scattering channel. As long as the hierarchy $\omega \ll T \ll \mu$ is maintained, where μ is the electronic chemical potential, this effect remains. We can interpret the situation as follows: the rotors are scattered by a static random magnetic field $\nabla\times\boldsymbol{a}(\boldsymbol{x})$, generated by the emergent gauge fluctuations, which increases the resistivity compared with the usual insulator-superfluid transition of rotors. The width of this random distribution of static magnetic fields is proportional to the temperature T. This is illustrated in Fig. 5. To determine the corresponding scattering rate, let us first rewrite the gauge-boson–rotor scattering term

$$\begin{aligned} I_a[f_s] = \frac{2}{N}\int_0^\infty \frac{d\Omega}{\pi}\int\frac{d^2q}{(2\pi)^2}(2\boldsymbol{k}\times\hat{\boldsymbol{q}})^2 \mathrm{Im}D(\Omega,q) \\ \times\Bigg\{\frac{(2\pi)\delta(\epsilon_k-\epsilon_{k+q}-\Omega)}{4\epsilon_k\epsilon_{k+q}}[f_s(\boldsymbol{k},t)[1+f_s(\boldsymbol{k}+\boldsymbol{q},t)] \\ \times[1+n(\Omega)] - f_s(\boldsymbol{k}+\boldsymbol{q},t)[1+f_s(\boldsymbol{k},t)]n(\Omega)] \\ + \frac{(2\pi)\delta(\epsilon_k-\epsilon_{k+q}+\Omega)}{4\epsilon_k\epsilon_{k+q}}[f_s(\boldsymbol{k},t)[1+f_s(\boldsymbol{k}+\boldsymbol{q},t)] \\ \times n(\Omega) - f_s(\boldsymbol{k}+\boldsymbol{q},t)[1+f_s(\boldsymbol{k},t)][1+n(\Omega)]]\Bigg\}. \end{aligned} \tag{27}$$

We have neglected the particle-antiparticle production term, the one with $\delta(\epsilon_k+\epsilon_{-k+q}-\Omega)$, because it requires an energy $\Omega > 2m$, which renders it subleading due to the suppression of dynamical gauge fluctuations. Linearizing yields the simple relaxational form

$$I_a = -\frac{s\boldsymbol{E}\cdot\boldsymbol{k}\varphi(k,\omega)}{\tau_a(k)} = -\frac{\delta f_s}{\tau_a(k)} \tag{28}$$

with the momentum-dependent scattering rate

$$\frac{1}{\tau_a(k)} = \frac{T}{N}\times\frac{8k^2}{\pi\epsilon_k}\int_0^1 dy\frac{y^2\sqrt{1-y^2}}{\Pi_b^{\mathrm{j}}(0,2ky)}. \tag{29}$$

This result for the scattering rate due to the emergent gauge bosons is valid for temperatures $T \ll \mu$. This *elastic* scattering rate obtained in the static regime is universal in the sense that it does not depend on the Fermi-surface information, such as k_F and v_F. It follows that we can express it in terms of a single-parameter scaling function

$$\frac{1}{\tau_a} = \frac{T}{N}F_a\left(\frac{k}{T}\right). \tag{30}$$

The exact momentum dependence can be determined numerically and is shown in Fig. 6. In evaluating Eq. (29), had one simply used the $T=\delta=0$ result $\Pi_b^{\mathrm{j}}(0,q)\sim q$, the rate would have vanished as $k\to 0$.

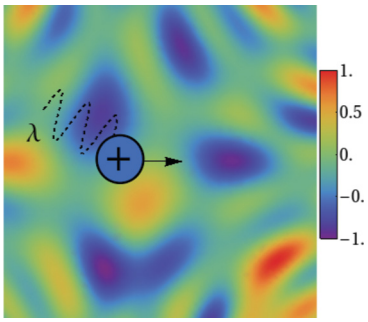

FIG. 5. (Color online) Illustration of the main scattering mechanisms determining the resistivity in the QC region. The blue disk corresponds to a holon excitation with charge $+e$. In addition to the usual scattering between critical charge fluctuations (mediated by the λ field), the static emergent gauge fluctuations generate a random "magnetic field" $\nabla\times\boldsymbol{a}$ that scatters the holons and doublons. A schematic configuration of this emergent magnetic field (which is always perpendicular to the plane) is shown, where the scale gives its strength and direction, the latter dictated by the sign.

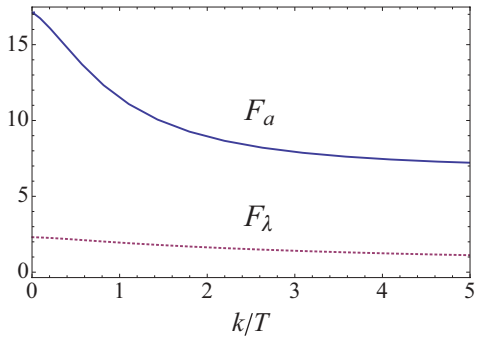

FIG. 6. (Color online) The scattering rate due to gauge fluctuations (solid line), Eq. (29), and due to the λ bosons (dashed line). The latter, F_λ, appears in Eq. (31) and is defined in Eq. (A3). We see that the rate due to the gauge fluctuations is a factor of ∼8 larger than that due to the λ field and is thus the dominant scattering mechanism.

After linearizing Eq. (24), we get the following equation for the deviation φ from the equilibrium distribution:

$$-i\omega\varphi(p,\omega) + g(p)/T^2 = \frac{T}{N}\left\{-[F_\lambda(p) + F_a(p)]\varphi(p,\omega) + \int dp' K_\lambda(p,p')\varphi(p',\omega)\right\}, \quad (31)$$

where we have Fourier transformed from time to frequency and have introduced dimensionless momentum variables p, p' that have been normalized by temperature: $p = k/T$. On the left-hand side, the term that makes the equation nonhomogeneous reads as $g(p) = \partial_{\epsilon_p} n(\epsilon_p)/\epsilon_p = -e^{\epsilon_p}/\epsilon_p(e^{\epsilon_p}-1)^2$, where it is understood that when we use the dimensionless momentum, the rotor mass is scaled by T, $\epsilon_p = \sqrt{p^2 + (m/T)^2}$, and the Bose function does not contain the usual factor of temperature: $n(\epsilon_p) = 1/(e^{\epsilon_p} - 1)$. We have also introduced the dimensionless kernel $K_\lambda(p,p')$ describing the nonelastic processes in which the rotors exchange energy with the λ bosons. It is independent of the gauge field, the driving frequency, and N. In analogy with Eq. (30), we have further defined the dimensionless function F_λ that corresponds to the scattering rate due to interactions with the λ field. More details about F_λ and K_λ can be found in Appendix A.

B. Solution of QBE and rotor conductivity

By performing the rescalings

$$\tilde{\omega} = \frac{\omega N}{T}, \quad (32)$$

$$\Phi(p,\tilde{\omega}) = \frac{T^3}{N}\varphi(p,\omega), \quad (33)$$

where again $p = k/T$ is the dimensionless momentum, we obtain a universal, parameter-free equation

$$-i\tilde{\omega}\Phi(p,\tilde{\omega}) + g(p) = -F(p)\Phi(p,\tilde{\omega}) + \int dp' K_\lambda(p,p')\Phi(p',\tilde{\omega}). \quad (34)$$

The gauge fluctuations do not spoil the existence of such a universal equation, which arises for the pure rotor theory,[21] because they contribute a universal scattering rate modifying $F_\lambda \to F_\lambda + F_a =: F$.

The above integral equation needs to be solved numerically. Once we obtain Φ, we can compute the low-frequency conductivity σ_{bI} from the expression for the current in terms of the distribution function of the rotors

$$\langle \boldsymbol{J}_I(\omega)\rangle = \int \frac{d^2k}{(2\pi)^2}\sum_{s=\pm} s\frac{\boldsymbol{k}}{\epsilon_k} f_s(\boldsymbol{k},\omega) \quad (35)$$

$$= \sum_s s\int \frac{d^2k}{(2\pi)^2}\frac{\boldsymbol{k}}{\epsilon_k} s\boldsymbol{E}\cdot\boldsymbol{k}\varphi(k,\omega). \quad (36)$$

Assuming the $\boldsymbol{E}$ field is in the x direction, we get

$$\sigma_{bI}(\omega) = \langle J_{Ix}(\omega)\rangle/E_x(\omega) \quad (37)$$

$$= \frac{1}{2\pi}\int_0^\Lambda dk\frac{k^3\varphi(k,\omega)}{\epsilon_k} \quad (38)$$

$$= N\times\frac{1}{2\pi}\int_0^{\Lambda/T} dp\frac{p^3\Phi(p,\tilde{\omega})}{\epsilon_p}, \quad (39)$$

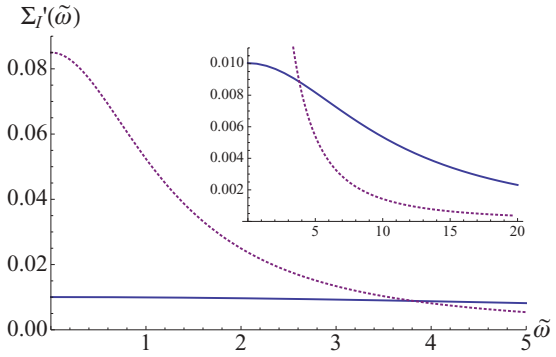

FIG. 7. (Color online) Universal scaling function for the real part of the conductivity above the QCP ($\delta = 0$). $\tilde{\omega} = N\omega/T$ is the rescaled frequency. The dotted line shows the scaling function in the absence of the gauge field. The inset shows Σ_I' for a larger range of $\tilde{\omega}$.

where Λ is the momentum cutoff used in the numerical solution. The last equality makes use of the scaling function for φ, so that the small-frequency conductivity $\omega/T \ll 1$ can be written as

$$\sigma_{bI}(\omega) = \frac{e^2}{\hbar}N\times\Sigma_I\left(\frac{N\omega}{T}\right), \quad (40)$$

where the fundamental constants e and $\hbar$ were reintroduced; Σ_I is a complex-valued universal function defined by Eq. (39), the real part of which is shown in Fig. 7. As shown there, the conductivity is substantially reduced *at small frequencies* $\tilde{\omega}$ compared with the pure $O(N)$ model due to the presence of the emergent gauge field. The universal number that determines the dc conductivity is $\Sigma_I(0) = 0.010$. It can be compared with $\Sigma_I^{O(N)}(0) = 0.085$ in the absence of the gauge field, i.e., for the pure $O(N)$ model. Extrapolating to the case of physical interest $N = 2$, the conductivity reads as

$$\sigma_b(0) = \frac{e^2}{\hbar}\times 0.020, \quad O(2) + \text{damped gauge field} \quad (41)$$

$$= \frac{e^2}{\hbar}\times 0.170, \quad \text{pure } O(2). \quad (42)$$

We note *en passant* that this last number for the pure $O(2)$ model, 0.170, is very close to what was obtained in the small-ϵ expansion,[22] 0.1650. Both these numbers lie near the self-dual value $1/2\pi \approx 0.159$ which is associated with a conductivity equal to the quantum of conductance e^2/h.

As the quantity that has a universal jump at the MIT is the resistivity and not the conductivity (unless we restrict ourselves to clean systems), we here give the expression for the rotor dc resistivity $\rho_b = 1/\sigma_b$:

$$\rho_b = \frac{\hbar}{e^2}R, \quad R = 49.8 \quad (43)$$

or $\rho_b = \frac{h}{e^2}\times 7.93 = 205\ \text{k}\Omega$. This constitutes one of our main results: the value of the universal resistivity jump estimated in the large-N approximation, as shown in Fig. 1.

Although the exact numbers can only be trusted in the large-N limit, we expect that some semiquantitative features are captured in our extension to $N = 2$. First, it is clear that the damped gauge field will necessarily make the conductivity smaller because it adds an additional scattering channel. The

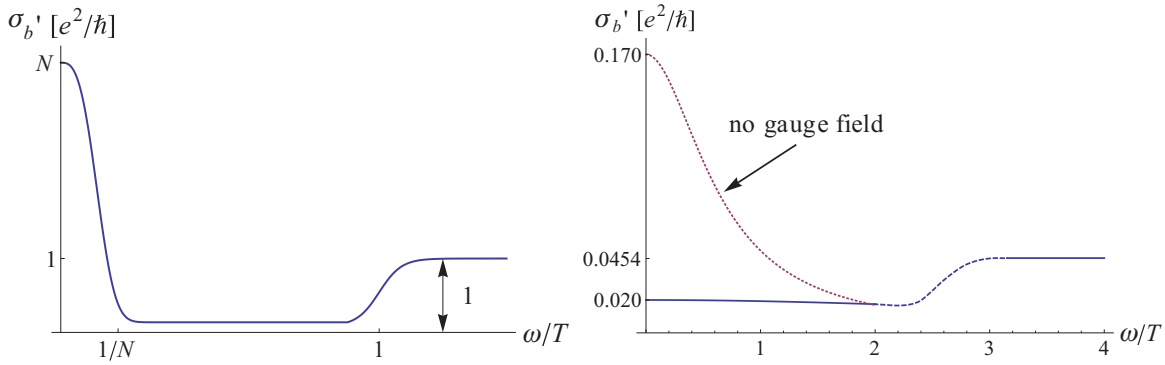

FIG. 8. (Color online) Frequency- and temperature-dependent rotor conductivity (real part). (a) Sketch of σ_b' in the large-N limit. There is a Drude-type peak of width $1/N$ and height N. While it is due to incoherent scattering of thermally excited quasiparticles, the large-frequency $\mathcal{O}(1)$ conductivity is from coherent and elastic scattering of field-excited carriers. (b) Large-N result extrapolated to $N = 2$, the case of physical interest for the Mott transition. The solid blue (dotted purple) line corresponds to the conductivity with (without) the emergent gauge field. The dashed line at intermediate frequencies is a sketch of the expected crossover to the high-frequency regime, where the gauge field becomes unimportant.

decrease in the rotor conductivity will lead to an increase in the resistivity, which translates into a bigger jump as one approaches the QCP from the metallic side, compared to a treatment that neglects gauge fluctuations. In our calculation, the increase is by a factor of ∼8, which is substantial. Although the actual enhancement might not be as large, our result suggests that the gauge fluctuations are the dominant source of current dissipation. Moreover, the strong scattering by the gauge bosons leads to the frequency dependence found in Fig. 8(b), where the Drude-type peak occurring in the pure $O(N)$ model disappears. Indeed, the small-frequency conductivity is smaller than in the $\omega/T \gg 1$ limit. This "inverse Drude peak" might naively suggest that vortex excitations, the conductivity of which is the quasiparticle *resistivity* $\sigma_b^{\text{vortex}} = \rho_b = 1/\sigma_b$ would be better suited, at least to describe electric transport. However, the vortices are known to give unreliable perturbative results for the superfluid-insulator transition in the pure $O(2)$ model. As the presence of the damped gauge boson does not alter the thermodynamic universality class, we suspect that this remains true in our model and that the dual vortex formulation does not offer any numerical advantage.

We briefly comment on the precise frequency dependence of the conductivity at low frequency, as shown in Fig. 7. It is possible to determine almost exactly the analytic form of this frequency dependence for both the pure and gauged $O(N)$ models,[30] which can be surprising given the complicated form of the QBE. Using the analytic expression, one can evaluate a low-frequency sum rule for the real part of the conductivity: $\int_0^\infty d\omega\, \sigma_b'(\omega) = \text{const}$. It is found that this integral equals the weight of the delta-function Drude peak obtained in the pure $O(N)$ NLσM at $N = \infty$, even in the presence of the gauge field. In particular, this means that the inclusion of the interactions at $1/N$ (λ or gauge boson mediated) only spreads the spectral weight of the delta function over a finite range of frequencies, this range being broader in the presence of the gauge field, as can be seen in the inset of Fig. 7.

V. CONDUCTIVITY IN THE ENTIRE QC REGION

We now examine how the conductivity changes as the system is tuned away from $g = g_c$ within the QC region, with $g \propto U/t$, the ratio of the Hubbard repulsion to the electronic bandwidth. The QC regions are defined by $T > \Delta_\pm$, where $\Delta_\pm$ are the two energy scales that vanish at the QCP. Δ_+, defined for $g > g_c$, is the Mott gap of the bosons, while Δ_-, $g < g_c$ is the phase stiffness of the rotors in their condensed phase. These two scales vanish approaching the QCP according to the power law

$$\Delta_\pm \sim |\delta|^{z\nu}, \tag{44}$$

where we are again using the signed energy scale associated with tuning the nonthermal parameter

$$\delta = g^{-1} - g_c^{-1} \propto t/U - (t/U)_c. \tag{45}$$

The dynamical exponent z is unity for all N, while the correlation length exponent ν depends on N: in the $N \to \infty$ limit, $\nu = 1/(d-1)$ so that in $d = 2$, $\nu = 1$. In the QC region, the effective mass of the rotors, the saddle-point value of the λ field, will change as δ is varied. This will naturally affect the conductivity: as one approaches the SL, the effective mass of the charge excitations increases and this leads to a larger electric resistivity. The mass will depend on the ratio of $\Delta_\pm/T$: $\frac{m}{T} = X_\pm(\frac{\Delta_\pm}{T})$. At $N = \infty$, we simply have $\Delta_\pm \propto |\delta|$, with the proportionality constants

$$\Delta_+ = 4\pi\delta, \quad g > g_c \tag{46}$$

$$\Delta_- = -\delta, \quad g < g_c. \tag{47}$$

There, an analytic solution can be obtained for the mass scaling function[31]

$$\frac{m}{T} = X\left(\frac{\delta}{T}\right), \tag{48}$$

$$X(\bar{\delta}) = 2\sinh^{-1}\left(\frac{e^{2\pi\bar{\delta}}}{2}\right), \tag{49}$$

which is plotted in Fig. 9.

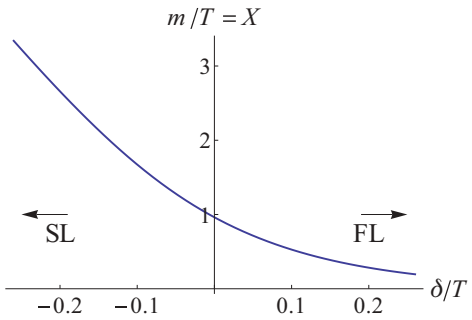

FIG. 9. (Color online) Rotor mass scaling function.

A. Results

We have solved for the frequency-dependent conductivity at different values of δ/T. The latter affects the polarization functions Π_b and Π_b^j via the rotor effective mass. The polarization functions determine the propagators of the λ and gauge boson, and thus the associated density of states the rotor excitations can scatter into. The universal scaling function for the low-frequency conductivity Σ_I was numerically obtained in the QC region:

$$\sigma_b = \frac{e^2}{\hbar} N \Sigma_I \left(\frac{N\omega}{T}, \frac{\delta}{T} \right). \tag{50}$$

In Fig. 10, we show the behavior of the corresponding dc resistivity extrapolated to $N = 2$: $\rho_b(0) = 1/\sigma_b(0) = (\hbar/e^2)/2\Sigma_I(0, \delta^{z\nu}/T)$. These numerical results should be compared with Fig. 3, where a sketch of the resistivity near the QCP was given, not restricted to the QC fan. It should also be compared with Fig. 15, in Appendix A, showing the rotor contribution without the gauge field, as relevant for the conventional superfluid-insulator transition. Let us first examine Fig. 10(c), which shows the resistivity along constant-δ cuts [Fig. 10(a)]. These curves can be naturally compared with sheet resistivity versus pressure experimental data, for instance, where $\delta \sim P - P_c$ plays the role of the deviation from the quantum critical pressure. As mentioned above, the rotor resistivity corresponds to the total electronic resistivity relative to the residual value in the FL: $\rho_b = \rho - \rho_m$. Curve 3 shows the resistivity at the critical pressure ($\delta = 0$): it is constant at low temperatures and takes a universal value $\frac{\hbar}{e^2} R$, with $R = 49.8$. As one goes down in temperature at pressures differing from P_c, the resistivity decreases approaching the FL (curves 4 and 5), or increases near the SL Mott insulator (curves 1 and 2). The more pronounced resistivity jump $\rho_b \to 0$ occurs upon exiting the critical Fermi surface state and going to the (marginal) FL, as is shown in Fig. 3(c). Figure 10(d) presents the results from a complementary perspective: by fixing T and tuning pressure following cuts shown in Fig. 10(b). This

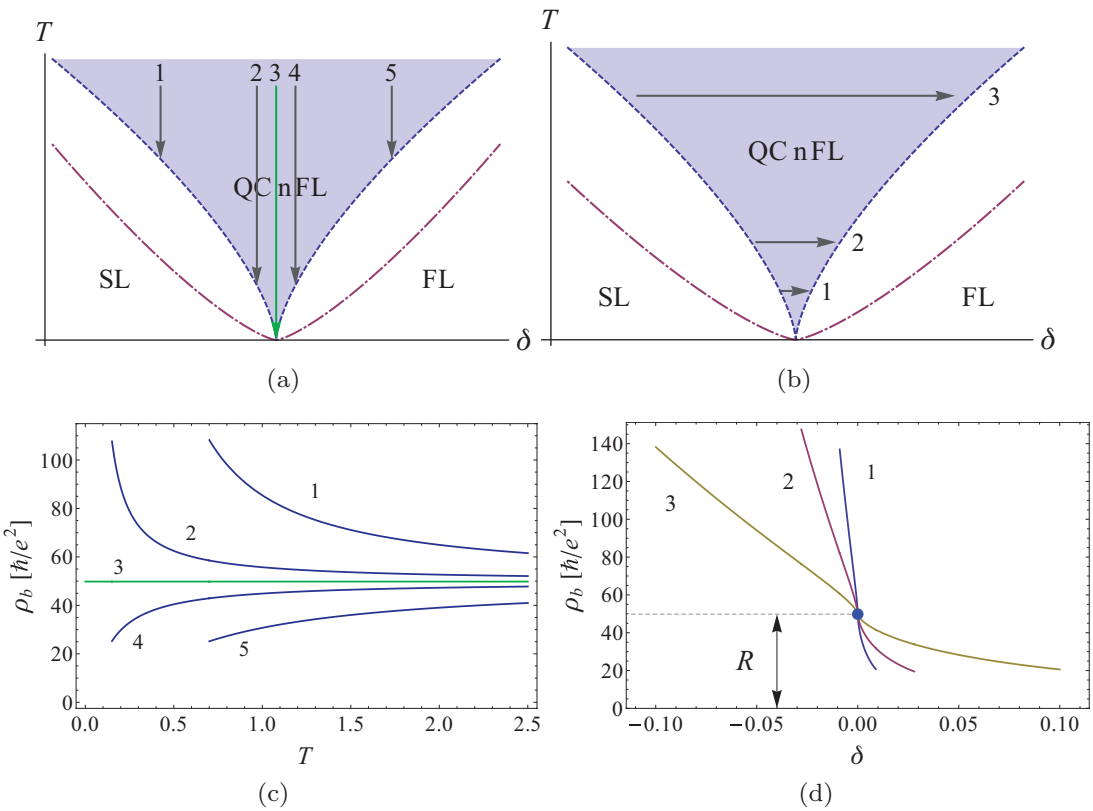

FIG. 10. (Color online) Behavior of the low-temperature dc resistivity near the quantum critical (QC) Mott transition as obtained from the solution of the quantum Boltzmann equation. Panel (c) shows the resistivity vs T for different ratios of the onsite repulsion over the bandwidth (tuned by δ). The corresponding cuts are shown in the phase diagram in (a) and correspond to $\delta = -0.01$, $-0.001, 0, 0.001, 0.01$ going from curve 1 to 5. Panel (d) shows the resistivity vs δ at different temperatures, with the corresponding cuts shown in the phase diagram in (b). Curves 1,2,3 correspond to $T = 0.5, 1.0, 2.5$, respectively. The universal rotor resistivity at criticality is $\rho_b = R\hbar/e^2$, with $R = 49.8$. (δ and T are given in a common and arbitrary unit of energy.)

illustrates how the $T = 0$ resistivity jump becomes smooth at finite temperature. By virtue of the scaling nature of the resistivity data, all curves cross at $\delta = 0$, where the resistivity is universal, $\frac{\hbar}{e^2}R$. The resistivity data was extracted from a single universal scaling function

$$\rho_b(\omega = 0) = \frac{\hbar}{e^2} G\left(\frac{\delta^{z\nu}}{T}\right). \tag{51}$$

We emphasize that, in experiments, it is the resistivity relative to its residual metallic value that should accordingly be examined for scaling in the vicinity of a quantum critical Mott transition. *Notes*: In obtaining the results shown in Fig. 10, we have replaced the $N = \infty$ scaling δ/T by the one appropriate for $N = 2$: $\delta^{z\nu}/T$, with $\nu = 0.67$ and $z = 1$ $\forall N$. [When $\delta < 0$, it is understood that $\delta^{z\nu} = \mathrm{sgn}(\delta)|\delta|^{z\nu}$.] A caveat with the extrapolation is that we have used the mass scaling function obtained at $N = \infty$. Although the specific form of $m/T = X(\delta^{z\nu}/T)$ will be different for $N = 2$, we expect it to be qualitatively similar, at least near criticality.

VI. CONDUCTIVITY AT LARGE FREQUENCIES AND TEMPERATURES

A. Large frequencies

In this section, we discuss the behavior of the rotor conductivity in the large-frequency limit $\omega \gg m \sim T$. As discussed above, in the large-N limit, the finite universal conductivity in that region mainly results from the elastic, coherent transport of charged excitations created by the external field, as opposed to the incoherent transport of thermally excited quasiparticles relevant at small frequencies. In our above treatment of the quantum Boltzmann equation, we can not obtain that part of the conductivity as we have neglected precisely those processes that are dominant for $\omega \gg T$. Rather, the large-frequency conductivity $\sigma_{bII} = (e^2/\hbar)\Sigma_{II}(\omega/T)$ can be obtained from a $T = 0$ calculation, i.e., in the limit $\omega/T \to \infty$. At $N = \infty$, the λ and gauge fields do not contribute and we recover the pure rotor contribution known from previous works,[28]

$$\Sigma'_{II}(\omega/T \gg 1) = \frac{\pi S_d}{2^d d}\left|\frac{\omega}{c}\right|^{d-2} \xrightarrow{d=2} \frac{1}{16} = 0.0625, \tag{52}$$

where $S_d = 2/[\Gamma(d/2)(4\pi)^{d/2}]$. Contrary to the dc conductivity, which was infinite at $N = \infty$, the fact that the high-frequency conductivity is already finite in the free limit testifies about the different mechanisms at play, namely, its collisionless nature in contrast to the hydrodynamic transport at small frequencies. Including the $1/N$ correction that arises due to interactions of the rotors with the λ field yields[28]

$$\Sigma'_{II}(\omega/T \gg 1) = \tfrac{1}{16}\left(1 - \tfrac{8}{3}\eta\right) \xrightarrow{N=2} 0.03998, \tag{53}$$

where $\eta = N^{-1}(8/3\pi^2)$ is the leading correction to the anomalous dimension of the rotor field. We do not include the gauge fluctuations because they are made "massive" by the Landau damping. At $T = 0$, even the static component is ineffective, lying within the continuum of dynamical excitations. For a more precise estimate of $\Sigma'_{II}(\infty)$, we quote the Monte Carlo results of Cha *et al.*,[28] i.e., $\Sigma'_{II}(\infty) = 0.0454$. This is the number we use for the large-frequency conductivity in Fig. 8(b).

B. Temperature dependence of electrical transport at criticality

In our analysis of the quantum critical resistivity, we have so far limited our discussion to the universal quantum critical resistivity of the bosons. As the temperature is decreased to zero right at the quantum critical point, how is this universal value approached? To address this we first note that the full resistivity at low T is given by the Ioffe-Larkin formula as the sum of boson and fermion resistivities. At low T, the dependence of the fermion resistivity is dominated by spinons scattering off the gauge fluctuations. As mentioned in Ref. 5, this leads to

$$\rho_f \sim \left(\frac{T}{\mu}\right)^2 \ln\left(\frac{\mu}{T}\right). \tag{54}$$

To obtain this dependence, the gauge propagator at criticality $D^{-1} \sim i\mu\frac{\omega}{v_F q} + q$ was used. Regarding the subleading temperature dependence of the rotor conductivity, we have indications (see next section) that the treatment of the QBE requires more care, as in the case of a Fermi surface of spinons coupled to an emergent gauge field.[32–34] We leave such analysis for future investigation. Notwithstanding, the leading nonconstant T dependence of the full resistivity will show a departure from the usual T^2 behavior because the rotor contribution is not expected to cancel the non-FL term provided by the spinons. This departure from a T^2 dependence constitutes a further signature of the non-FL nature of the critical Fermi-surface state. We note that the logarithmic correction due to the spinons will persist in the MFL phase because the gauge field only becomes Higgsed by the rotor condensate at lower temperatures, where the usual FL is recovered.

1. *Necessity of careful treatment of subleading T dependence of rotor conductivity*

To estimate the temperature dependence of the rotor conductivity at $\delta = 0$ beyond its universal constant value, one can try to compute the transport scattering rate, just as was done for the spinon contribution [Eq. (54)]. We need to evaluate the imaginary part of the rotor self-energy due to the gauge fluctuations, with the usual additional factor of $1 - \cos\theta$ in the integrand. The leading-order dependence is universal and linear in T, in agreement with our QBE calculation. The subleading term is negative and goes like $-T^2/\mu$, where μ is the fermionic chemical potential. We believe that such a negative contribution points to the inability of such a simple approach to capture the correct T dependence. Indeed, this scattering rate would imply a conductivity that increases with temperature via $\sigma_b \sim T\tau_{\mathrm{tr}}^b \sim 1/(1 - T/\mu)$.

Instead of using this semiclassical approach, we can turn to the full quantum Boltzmann equation. However, a straightforward approach fails because the QBE contains terms that diverge due to scattering of low-energy gapless gauge bosons. This can be related to the divergence of the rotor self-energy at finite T, which displays a logarithmic singularity in the infrared. It can not be naively cut off because the low-energy properties of the gauge field and rotors were properly treated. This situation is exactly analogous to the case of fermionic spinons or nonrelativistic bosons coupled to an emergent gauge field studied in the context of U(1) spin liquids.[32] It was found that the divergence of the self-energy

(or vanishing of the Green's function) is a natural consequence of the gauge fluctuations on a non–gauge-invariant operator, which in this case is the rotor Green's function.

This type of singularity in the QBE was previously encountered in the context of the spinon–gauge-field problem by Kim *et al.*,[33] revisited latter by Nave and Lee.[34] Kim *et al.* found that a separation of the gauge fluctuations into static (with frequency less than the temperature) and dynamic ones together with the use of a gauge-invariant momentum remove the singularities and allow the extraction of physical quantities. It was also noted that the static gauge fluctuations act as a random magnetic field that contributes to the conductivity by increasing the scattering of spinons, a situation very analogous to the effects of the gauge field on the critical rotors analyzed in this work. However, in the present system, the static gauge fluctuations dominate the low-temperature transport and we did not need to take into account the dynamical or quantum gauge fluctuations, at least for the low-temperature transport. The latter are essential to determine the higher-temperature behavior and one needs to perform a careful treatment analogous to Ref. 33, a task we leave for the future.

VII. THERMAL CONDUCTIVITY

The thermal conductivity also bears a signature of the critical Fermi surface, in which the emergent gauge field plays an even more important role than for electric transport. According to the Ioffe-Larkin composition rule, the thermal *conductivities* of the spinons and rotors add[32] $\kappa = \kappa_b + \kappa_f$. In other words, the thermal resistivities add in parallel, which is in contrast to the rule for electrical resistivity (addition in series) because of the absence of charge flow in response to the thermal gradient. In this sense, the thermal current is oblivious to the slave-rotor constraint relating the rotor charge to the spinon number, and the *relative* flow of the partons can proceed unconstrained.

Let us first consider the rotor thermal conductivity κ_b. In the absence of the gauge field, the rotors decouple from the spinons and their action reduces to the critical theory of the pure $O(N)$ model. This is a conformal field theory (CFT). On symmetry grounds, a CFT has infinite thermal conductivity because the energy current is conserved.[35,36] Indeed, by virtue of conformal invariance, there exists a conserved and symmetric energy-momentum tensor: $\partial_\mu T_{\mu\nu} = 0$ and $T_{\mu\nu} = T_{\nu\mu}$, where μ,ν are space-time indices. These two conditions imply that $\frac{d}{d\tau}\int d\boldsymbol{x}\ T_{i\tau} = 0$, with spatial indices $i = x,y$. Put in words, the energy current $T_{i\tau}$ is conserved and will not be dissipated by interactions, contrary to the charge current. In our critical theory, this situation is avoided because of the damped gauge fluctuations, which naturally break conformal invariance and lead to a finite and universal critical thermal conductivity:

$$\kappa_b = \frac{k_B^2}{\hbar} K T\,, \tag{55}$$

where K is a dimensionless number associated with the Mott QCP, just like R. The gauge fluctuations are more detrimental in the determination of the thermal conductivity than for the electric conductivity: whereas the latter was already a finite universal constant without the gauge bosons, the former is formally infinite without the gauge fluctuations. In reality, this would not be the case due to the presence of irrelevant (in the RG sense) umklapp scattering by the lattice, which would lead to a large, nonuniversal but finite conductivity. In the case under consideration, we do not need to refer to such processes because the gauge scattering is stronger and leads to a universal answer [Eq. (55)].

Although the full calculation of κ_b is beyond the scope of this work, we mention some of the important aspects. First, in the electric resistivity calculation performed above, a key simplification in the large-N framework is that we can neglect the effect of the electric field on the λ. As was explained in Sec. IV A, only one rotor flavor is directly coupled to the electric field so that its effects on the rotor polarization functions, which are obtained by summing over all rotor flavors, are subleading in N. This is no longer true when a thermal gradient is present, as all rotor flavors inexorably transport energy/entropy in the same way. Hence, the nonequilibrium corrections to the polarization functions can not be neglected. To obtain the correct QBE describing the heat transport, one should use the Keldysh formalism, a task beyond the scope of this work.

We now turn to the spinon conductivity κ_f. In the presence of weak disorder, the low-temperature spinon thermal conductivity will scale like $\kappa_f = \text{const} \times T$, a form valid on both sides of the transition. Approaching from the FL, the constant κ/T is simply $L\sigma_m$, where $L = \frac{\pi^2}{3}(\frac{k_B}{e})^2$ is the usual Lorentz number, while σ_m is the residual metallic conductivity, by virtue of the Wiedemann-Franz law obeyed in the FL. As the critical point is reached, κ/T jumps by a universal amount $\frac{k_B^2}{\hbar}K$. Note that contrary to the electric conductivity, the thermal one is finite on the SL side, and is dominated by the spinon–gauge-field sector.

A. Violation of Wiedemann-Franz

Combining the electric resistivity and κ/T jumps, we predict the Lorenz number $L = \kappa/T\sigma = \rho\kappa/T$ will also jump at the transition, indicating a violation of the Wiedemann-Franz law. In the clean limit, the violation is drastic as the Lorenz number will actually diverge directly at the transition because the electric conductivity is finite but the thermal one is infinite due to the spinon Fermi surface. The violation is even worse in the SL where the conductivity also vanishes. In the presence of weak disorder, as is more relevant for experiments, the thermal conductivity will be finite throughout, in particular at the QCP, and this will lead to a universal jump by an amount $KR(k_B/e)^2$, where K and R are the universal numerical coefficients of the thermal conductivity (divided by T) and resistivity of the critical rotors. We emphasize that this $T = 0$ universal jump will become a rapid increase at finite T, just as happens in the case of the resistivity. We finally note that the Lorenz number will take the usual free-fermion value in the FL, $L = (\pi^2/3)(k_B/e)^2$, because elastic scattering by impurities dominates at small energies. In the clean limit, the actual numerical coefficient of L in the FL is expected to differ from $\pi^2/3$ because of the frequency dependence of the interaction-induced scattering rate.[37] However, we emphasize that what is important is the *relative* jump at the QCP.

VIII. DISCUSSION

A. Experiments

A preliminary analysis of unpublished pressure- and temperature-dependent resistivity data on both κ-(BEDT-TTF)$_2$Cu$_2$(CN)$_3$ (Ref. 38) and EtMe$_3$Sb[Pd(dmit)$_2$]$_2$ (Ref. 39) provide encouraging hints regarding the presence of a quantum critical Mott transition as described in this work. Indeed, at sufficiently high temperatures, the *sheet resistivity* saturates to a constant $\sim 10h/e^2$, as we predict. The qualitative pressure and temperature dependencies are also roughly in agreement with our results. A closer analysis of the data will be needed to make a stronger statement, not to mention the potential complications with the inhomogeneous effects of pressure on the relatively soft organic salts.

B. Disorder

We discuss the effects of disorder and provide an estimate for the temperature at which we expect it to become important in the context of the organics. We shall assume the disorder is weak as is appropriate for these materials. Then, its main effect will be to modify the gauge field's inverse Green's function to (we work in imaginary time)

$$k_F \frac{|\Omega_n|}{\sqrt{q^2 + 1/l^2}} + \sigma_b^\infty \sqrt{\Omega_n^2 + c^2 q^2}. \tag{56}$$

Here, l is the spinon elastic mean-free path, and we have reinstated c, the rotor velocity, which is on the order of v_F. σ_b^∞ is a shorthand for the $T = 0$ rotor conductivity $\sigma_b(\omega/T \gg 1)$. The zero Matsubara frequency gauge mode does not respond to the change in the Landau damping, which vanishes at zero frequency. So, the question is about the effect on the nonzero Matsubara frequency components. These will notice the finite mean-free path when $q < 1/l$ or relating the gauge boson energy ($\sim T$) to the momentum via the $z = 2$ scaling $\Omega \sim q^2$, we get $T \lesssim \frac{\sigma_b^\infty c}{k_F l^2}$. Using $c \approx v_F$, this can be cast as

$$T \lesssim \frac{\sigma_b^\infty \mu}{(k_F l)^2}, \tag{57}$$

where μ is the Fermi energy or chemical potential. The organics are good metals, so we take $k_F l \approx 10$, although the actual mean-free path is probably larger. Also, $\mu \approx 10^3$ K and $\sigma_b^\infty \approx 0.05$, in units of $e^2/\hbar$. We thus conclude that within our framework, using parameters relevant to the organics of interest, disorder will start playing an important role at temperatures

$$T \lesssim 0.5\,\mathrm{K}. \tag{58}$$

Above that temperature, we can treat the higher Matsubara modes without including disorder, and the results of this paper should provide a valid description.

IX. CONCLUSION

We have analyzed the transport signatures of a quantum critical Mott transition between a Fermi-liquid metal and a paramagnetic Mott insulator in two spatial dimensions, at fixed filling. In this scenario, the Mott phase is characterized by a Fermi surface of spin-only quasiparticles, resulting in a gapless U(1) spin liquid. The physics of such a transition is conveniently captured by a slave-rotor field theory of the electronic Hubbard model, in which the charge fluctuations are described by a quantum XY model of rotors, coupled to an emergent gauge field. The superfluid phase of the rotors corresponds to the metal, while a Mott insulator results in the disordered phase, where only spin fluctuations remain gapless. Directly at the transition, a strongly correlated non-Fermi-liquid metal emerges where the electronic Fermi surface is on the brink of disappearance; it is an instance of a critical Fermi surface. The zero-temperature electric resistivity of such a critical state was predicted to be greater than that of the Fermi liquid by a universal amount $R\hbar/e^2$, where R is a dimensionless number associated with the Mott quantum critical point (see Fig. 1). We have obtained an estimate for this number, $R \approx 49.8$, via the solution of a quantum Boltzmann equation for the charge fluctuations, analyzed in a large-N limit. We found that the emergent gauge fluctuations strongly contribute to the universal resistivity jump, albeit being ineffective at changing the universality class of the charge fluctuations from 3D XY. This is so because the *static* gauge fluctuations escape the Landau damping, and are responsible for the strong, and universal, scattering of the critical charge fluctuations. Although we have focused on transport properties which are best accessed in experiments, we may anticipate that the static gauge-field fluctuations might also affect other dynamical quantities (for instance, the low-frequency form of the electron self-energy at nonzero temperature) in the quantum critical regime.

We have further examined how this resistivity jump evolves at finite temperature and as one changes the ratio of the Hubbard repulsion to the electronic bandwidth (experimentally tunable by applying pressure). We have obtained a universal scaling function that can be used to collapse the temperature- and pressure-dependent resistivity in the quantum critical Fermi-surface state: $\rho - \rho_m = (\hbar/e^2) G(\delta^{z\nu}/T)$, where ρ_m is the residual resistivity in the Fermi liquid, δ can be mapped to the deviation from the critical pressure, and z and ν are the usual dynamical and correlation length exponents, respectively, of the 3D XY universality class. In particular, $G(0) = R$.

Turning to thermal transport, we make the prediction that the low-temperature thermal conductivity (divided by temperature) κ/T has a universal jump at the transition (Fig. 1). The gauge fluctuations are responsible for this jump by breaking the conformal invariance of the charge fluctuations. Together with the jump of the electric resistivity, the thermal conductivity jump leads to a violation of the Wiedemann-Franz law by the critical Fermi-surface state.

Regarding experiments, the organic salts κ-(BEDT-TTF)$_2$Cu$_2$(CN)$_3$ and EtMe$_3$Sb[Pd(dmit)$_2$]$_2$ are candidate materials for the transition covered in this work. Indeed, at ambient pressure they display numerous signatures characteristic of a gapless quantum spin liquid, and become metallic under the application of hydrostatic pressure. As mentioned in Sec. VIII, recent unpublished data for the temperature- and pressure-dependent resistivity near the Mott transition seem to indicate a jump on the order of h/e^2 near the transition,

as well as qualitative agreement with the scaling we propose. A confirmation would point towards the first experimental example of a quantum critical Mott transition (of fermions), as well as a nontrivial signature of spin-charge separation in two dimensions.

On the theoretical side, it would be interesting to investigate the charge transport within a controlled dimensional expansion, with small parameter $3-d$ where d is the spatial dimension, and see how the results compare with the large-N expansion. Numerical simulations directly in $d=2$ and at $N=2$ would also be desired. Regarding the jump of the thermal conductivity, a full treatment within the large-N expansion is still missing due to the complication of drag of the constraint field of the $O(N)$ nonlinear sigma model. A first step would be to establish the divergence of the thermal conductivity in the pure XY model, as required by conformal invariance, then to include the emergent gauge fluctuations. Taking a broader perspective, we envision that the results regarding the effects of the damped gauge fluctuations on the transport of relativistic or particle-hole–symmetric quasiparticles discussed in this work can be applied to other systems.

ACKNOWLEDGMENTS

We are very grateful for many insightful discussions with S. Sachdev, and for his assistance in helping verifying numerical results for the pure $O(N)$ model. We are indebted to K. Kanoda and R. Kato for sharing their unpublished data, and for enlightening discussions. We also wish to thank K. Damle for early discussions and for providing a copy of his Ph.D. thesis, as well as A. G. Green for sharing his knowledge of the thermal response of relativistic bosons. Finally, we acknowledge insightful discussions with M. Barkeshli, L. Fritz, S.-S. Lee, K. Michaeli, L. Motrunich, D. Mross, A. Paramekanti, D. Podolsky, A. Potter, J. Rau, G. Refael, and X.-G. Wen. We acknowledge the hospitality of MIT (W.W.K.) and Perimeter Institute (T.S., W.W.K.), where significant portions of this work were done. This research was funded by NSERC, the Canada Research Chair program, and the Canadian Institute for Advanced Research (W.W.K., Y.B.K.), FQRNT and the Walter Sumner Foundation (W.W.K.), an ICMT fellowship at UIUC (P.G.), and NSF Grant DMR-1005434 (T.S.).

APPENDIX A: TRANSPORT IN THE PURE $O(N)$ ROTOR THEORY

In this Appendix, we present details regarding transport properties of the pure $O(N)$ NLσM, where the $N=2$ theory describes the superfluid-insulator transition of bosons in two dimensions, as present in the Bose-Hubbard model at integer filling for instance. Some of these results correct previous ones, or can not be found in the literature. In addition, they are important as a comparison ground with the rotor theory used to describe charge criticality in the Mott transition under consideration. The latter is a gauged version of the $O(N)$ model, with a Landau damped gauge boson.

The bare action for the pure $O(N)$ theory is

$$S_b = \frac{1}{2g}\int_x \left(|\partial_\nu b_\alpha|^2 + i\lambda(|b_\alpha|^2-1)\right), \tag{A1}$$

where α runs from 1 to $N/2$, so that the $N/2$ complex fields form a real $O(N)$ vector field. The above action has full $O(N)$ global invariance. (The notational choice of using $N/2$ complex fields instead of N real ones is more convenient from the point of view of the slave-rotor formulation.) Again, λ is a Lagrange multiplier field enforcing the constraint that the rotor is unimodular: $\sum_\alpha |b_\alpha| = 1$. In the $N=\infty$ limit, the field theory becomes free, allowing a $1/N$ perturbative expansion. At $N=\infty$, the expectation value of the λ field plays the role of an effective mass for the rotors in their insulating phase, as described in Sec. III. The saddle-point equation for λ is still given by Eq. (12) because the fluctuating gauge field does not affect the $N=\infty$ rotors. In the symmetry-broken phase, the saddle-point equation for the effective mass has no solution, indicating long-range order (at $T=0$ only for $N>2$).

We now turn to the charge transport near the quantum critical point. Out of the many charges present at large N, we couple the electric field to a single one, say the complex component b_1. We focus on the regime where the external field has a small driving frequency compared with temperature; this corresponds to the collision-dominated hydrodynamic regime. At $N=\infty$, the dc conductivity is infinite because interactions are entirely suppressed in that limit. At order $1/N$, the λ field acquires a nonzero propagation amplitude and can scatter the positive and negative charge excitations, the holons and doublons, respectively. The quantum Boltzmann equation for the holons and doublons can be read off Eq. (24), where one simply has to set the gauge propagator $\propto D(\Omega,q)$ to zero. As explained in the main text, we expand the holon and doublon distribution functions to linear order in the electric field: $f_\pm(\boldsymbol{k},\omega) = 2\pi\delta(\omega)n(\epsilon_k) \pm \boldsymbol{E}\cdot\boldsymbol{k}\varphi(k,\omega)$. Linearizing the QBE, we obtain

$$\begin{aligned} &-i\omega\varphi(p,\omega) + g(p)/T^2 \\ &\quad = \frac{T}{N}\left\{-F_\lambda(p)\varphi(p,\omega) + \int dp'\, K_\lambda(p,p')\varphi(p',\omega)\right\}, \end{aligned} \tag{A2}$$

which is the same as Eq. (31), except that we have set the scattering rate due to gauge fluctuations F_a to zero. As before, $g(p) = \partial_{\epsilon_p} n(\epsilon_p)/\epsilon_p$. The functions F_λ and K_λ can be written in the simple form

$$\begin{aligned} F_\lambda(p) = \int_0^\infty \frac{p'dp'}{2\pi}\frac{1}{\epsilon_p\epsilon_{p'}}&[\mathcal{A}(p,p')|\gamma(p,p')| \\ &+ \mathcal{A}_{\rm dh}(p,p')\gamma_{\rm dh}(p,p')], \end{aligned} \tag{A3}$$

$$\begin{aligned} K_\lambda(p,p') = \frac{p'}{2\pi}\frac{1}{\epsilon_p\epsilon_{p'}}&[\mathcal{A}_{\rm c}(p,p')|\gamma(p',p)| \\ &- \mathcal{A}_{\rm c,dh}(p,p')\gamma_{\rm dh}(p',p)]\frac{p'}{p}, \end{aligned} \tag{A4}$$

where we have defined the two γ functions

$$\gamma(p,p') = n(\epsilon_{p'}-\epsilon_p) - n(\epsilon_{p'}) = \frac{1-e^{-\epsilon_{p'}}}{(1-e^{-\epsilon_p})(1-e^{\epsilon_p-\epsilon_{p'}})}, \tag{A5}$$

$$\gamma_{\rm dh}(p,p') = n(\epsilon_{p'}) - n(\epsilon_p+\epsilon_{p'}) \tag{A6}$$

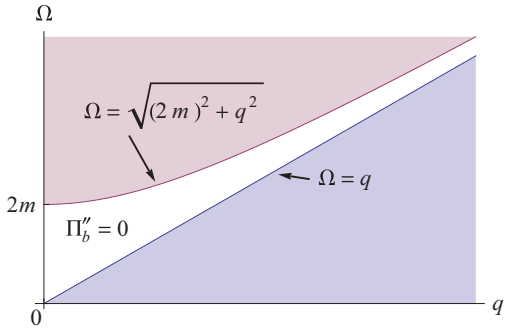

FIG. 11. (Color online) The shaded regions correspond to $\Pi_b'' \neq 0$. The upper one (purple) is due to the on-shell pair production of holons and doublons, each with mass m.

and the four $\mathcal{A}$ functions

$$\mathcal{A}(p,p') = \int_0^{2\pi} \frac{d\theta}{2\pi} A(|\epsilon_p - \epsilon_{p'}|, |\boldsymbol{p} + \boldsymbol{p}'|), \quad \text{(A7)}$$

$$\mathcal{A}_c(p,p') = \int_0^{2\pi} \frac{d\theta}{2\pi} A(|\epsilon_p - \epsilon_{p'}|, |\boldsymbol{p} + \boldsymbol{p}'|)(-\cos\theta), \quad \text{(A8)}$$

$$\mathcal{A}_{dh}(p,p') = \int_0^{2\pi} \frac{d\theta}{2\pi} A(\epsilon_p + \epsilon_{p'}, |\boldsymbol{p} + \boldsymbol{p}'|), \quad \text{(A9)}$$

$$\mathcal{A}_{c,dh}(p,p') = \int_0^{2\pi} \frac{d\theta}{2\pi} A(\epsilon_p + \epsilon_{p'}, |\boldsymbol{p} + \boldsymbol{p}'|)(-\cos\theta), \quad \text{(A10)}$$

where θ is the angle between $\boldsymbol{p}$ and $\boldsymbol{p}'$. We have also defined the scaled spectral function of the λ field: $A(\Omega,q) = -\mathrm{Im}[1/\Pi_b(\Omega,q)]$, where the factor of $2/N$ in the λ propagator $2/N\Pi_b$ was omitted from the definition of A. The sign of A is such that $A(\Omega > 0, q) > 0$. The $\mathcal{A}$ functions can be readily seen to be positive and symmetric. The "c" indicates a cosine in the angle integral, while "dh" stands for doublon-holon. To understand this last piece of notation, we need to examine Π_b, specifically its imaginary part:

$$\Pi_b''(\Omega,q) = \int \frac{d^2k}{16\pi\epsilon_k\epsilon_{k+q}} \{|n(\epsilon_{k+q}) - n(\epsilon_k)|\delta(|\epsilon_{k+q} - \epsilon_k| - \Omega) + [1 + n(\epsilon_k) + n(\epsilon_{k+q})]\delta(\epsilon_k + \epsilon_{k+q} - \Omega)\}, \quad \text{(A11)}$$

which is nonzero in two separate regions, a low- and high-energy one: $\Omega < q$ and $\Omega > \sqrt{(2m)^2 + q^2}$, respectively, as is illustrated in Fig. 11. The latter region arises from the production of holon-doublon pairs, which requires an energy beyond a certain threshold. The λ-boson spectral function has support in the same regions, being proportional to Π_b'': $A = -\mathrm{Im}[1/\Pi_b] = \Pi_b''/[(\Pi_b')^2 + (\Pi_b'')^2]$. We plot the numerically evaluated spectral function in Fig. 12. We note that A vanishes at the boundaries of the region where $\Pi_b'' = 0$. Going back to the $\mathcal{A}$ functions, it can be seen that those labeled "dh" receive contributions precisely from the doublon-holon pair production region.

By performing the rescaling $\tilde{\omega} = \omega N/T$ and

$$\Phi(p,\tilde{\omega}) = \frac{T^3}{N}\varphi(p,\omega), \quad \text{(A12)}$$

we obtain a universal, parameter-free equation

$$-i\tilde{\omega}\Phi(p,\tilde{\omega}) + g(p) = -F_\lambda(p)\Phi(p,\tilde{\omega}) + \int dp' K_\lambda(p,p')\Phi(p',\tilde{\omega}). \quad \text{(A13)}$$

We solve the integral equation numerically by discretizing the momentum variables and expanding the unknown function Φ in terms of Chebyshev polynomials. This procedure converts the integral equation into a matrix equation, which is solved by simply inverting the matrix corresponding to the kernel K_λ. We plot the solution in Fig. 13. $\Phi(p,\tilde{\omega})$ goes to a constant as $p \to 0$ and decays exponentially for $p \gg 1$, i.e., for momenta much greater than the temperature. Also, as the driving frequency $\omega \propto \tilde{\omega}$ goes to zero, the imaginary part Φ'' vanishes as expected since the dc conductivity is purely real.

The resulting frequency-dependent conductivity can be obtained by integrating $\Phi(p,\tilde{\omega})$ over momentum, as shown in Eq. (39). As a result, we obtain a scaling function for the conductivity: $\sigma_b = (e^2/\hbar)N\Sigma_I(\tilde{\omega}, \delta^{zv}/T)$. The numerical solution for the scaling function is shown in Fig. 14, where (a) shows the frequency dependence of both the real and imaginary parts of the scaled conductivity for $\delta = 0$, while (b) shows the real part away from criticality at five different values of δ/T. Figure 14(b) shows that the conductivity increases going away from the disordered to the symmetry-broken

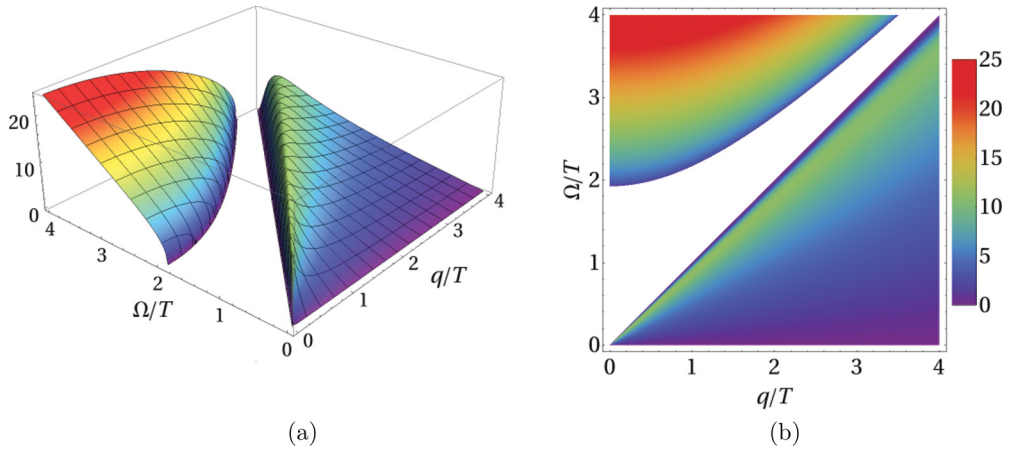

FIG. 12. (Color online) (a) Spectral function for the λ bosons: $A(\Omega,q) = -\mathrm{Im}[1/\Pi_b(\Omega,q)]$. (b) The corresponding density plot.

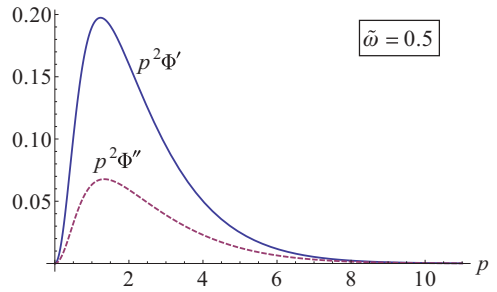

FIG. 13. (Color online) Solution for electric-field-induced deviation to the rotor distribution function $\Phi(p,\tilde{\omega})$ for $\tilde{\omega} = N\omega/T = 0.5$. The solid (dashed) line shows the real (imaginary) part, multiplied by p^2.

phase, corresponding to sweeping δ from negative to positive values.

For $N = 2$, the conductivity is given by $\sigma_b = (e^2/\hbar)2\Sigma_I(2\omega/T, \delta^{zv}/T)$, so that the curves in Fig. 14 give the conductivity (in units of $2e^2/\hbar$) versus $2 \times \omega/T$. In general, the scaled frequency $\tilde{\omega}$ on the horizontal axis should be multiplied by $1/N$ to get the dependence on ω/T. In the large-N limit, we recover a Drude-type peak, as the charged quasiparticles interact more weakly. As mentioned at the end of Sec. IV B, the essentially exact frequency dependence of the small-frequency conductivity [cf. Fig. 14(a)] was recently determined.[30] This result can be used to prove a sum rule constraining the integral of the real part of the conductivity to the weight of the delta-function Drude peak at $N = \infty$, i.e., in the free limit of the theory. This provides an excellent check on the numerics.

Focusing on $N = 2$, Fig. 15 shows the behavior of the resistivity in the QC region. We have indicated the presence of a Kosterlitz-Thouless transition by a solid line at the interface between the QC regime and the SF. For $N > 2$, this finite-T phase transition is converted to a crossover. This figure should be compared with Fig. 10, where there the bosons are coupled to a Landau damped gauge field. We see that not only does the gauge field make the resistivity larger, but its variations are also more pronounced as δ and T are changed.

APPENDIX B: THERMAL CONDUCTIVITY

We discuss some aspects of the thermal conductivity of the rotors. In particular, via the solution of a QBE, we explicitly show that in the absence of gauge fluctuations, the rotors have infinite thermal conductivity, as expected based on conformal invariance. We then go on to argue that with the addition of the damped gauge field, the conductivity becomes finite, specifically $\kappa_b = (k_B^2/\hbar)KT$, where K is a dimensionless constant. In the large-N formulation, one needs to include effects of the thermal gradient on the constraint field λ, complicating the analysis. We thus consider an alternate but equivalent formulation of the critical theory where the hard constraint of the XY rotor model $|b| = 1$ is traded for a soft one via the addition of quartic term $|b|^4$.

1. Thermal response of pure $O(2)$ model: CFT and zero modes

The critical theory for the "soft" rotor model, without gauge field, is described by the action

$$S = \frac{1}{2}\int d^{d+1}x\, |\partial_v b|^2 + m^2|b|^2 + \frac{u}{12}|b|^4\,, \qquad \text{(B1)}$$

where $d = 3 - \varepsilon$ is the space-time dimension, and $m^2 = \varepsilon(4\pi^2/15)T^2$ and $u = \varepsilon(24\pi^2/5)$. This is the standard Wilson-Fisher fixed point resulting from a perturbative RG treatment (see, e.g., Ref. 22, which studies the electric transport properties of that model). We have thus traded the large-N expansion for a dimensional expansion in ε, $N = 2$ being fixed.

We are interested in the linear response of the bosons to a thermal gradient. As we did above in the case of the electric transport, we consider the QBE for the holon and doublon distribution functions $f_\pm$. The static thermal gradient is imposed by including a position-dependent temperature $T(\boldsymbol{x})$, which in turn generates position dependence for the distribution functions $f_\pm$. The corresponding QBE, which can be found in Refs. 40 and 41, reads as

$$\boldsymbol{v}_k \cdot \frac{\partial f_\pm}{\partial \boldsymbol{x}} = I_\pm[f_+, f_-]\,, \qquad \text{(B2)}$$

where $\boldsymbol{v}_k = \partial\epsilon_k/\partial\boldsymbol{k}$ and $\epsilon_k = \sqrt{k^2 + m^2}$. The collision term is different from the large-N expansion as it arises from the

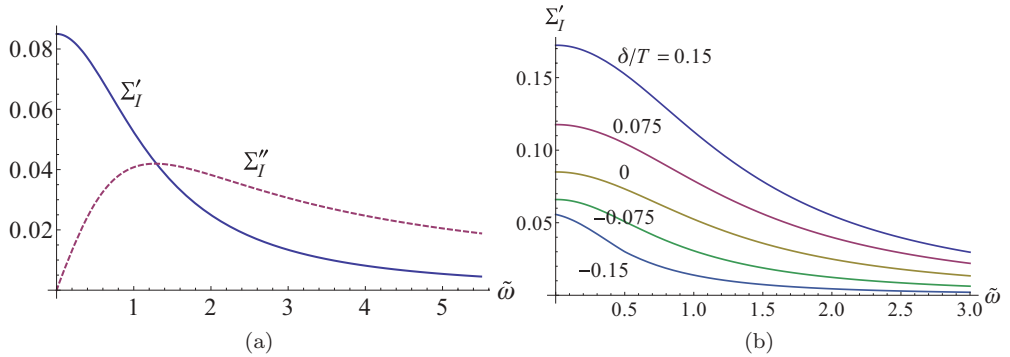

FIG. 14. (Color online) Conductivity universal scaling function for the pure $O(N)$ theory. (a) Frequency-dependent scaling at finite T above the QCP $\delta = 0$: $\sigma_b = N\Sigma_I(\tilde{\omega})$, where the argument is $\tilde{\omega} = N\omega/T$. The solid (dashed) line corresponds to the real (imaginary) part. (b) The scaling function (real part) as a function of the departure from criticality δ/T.

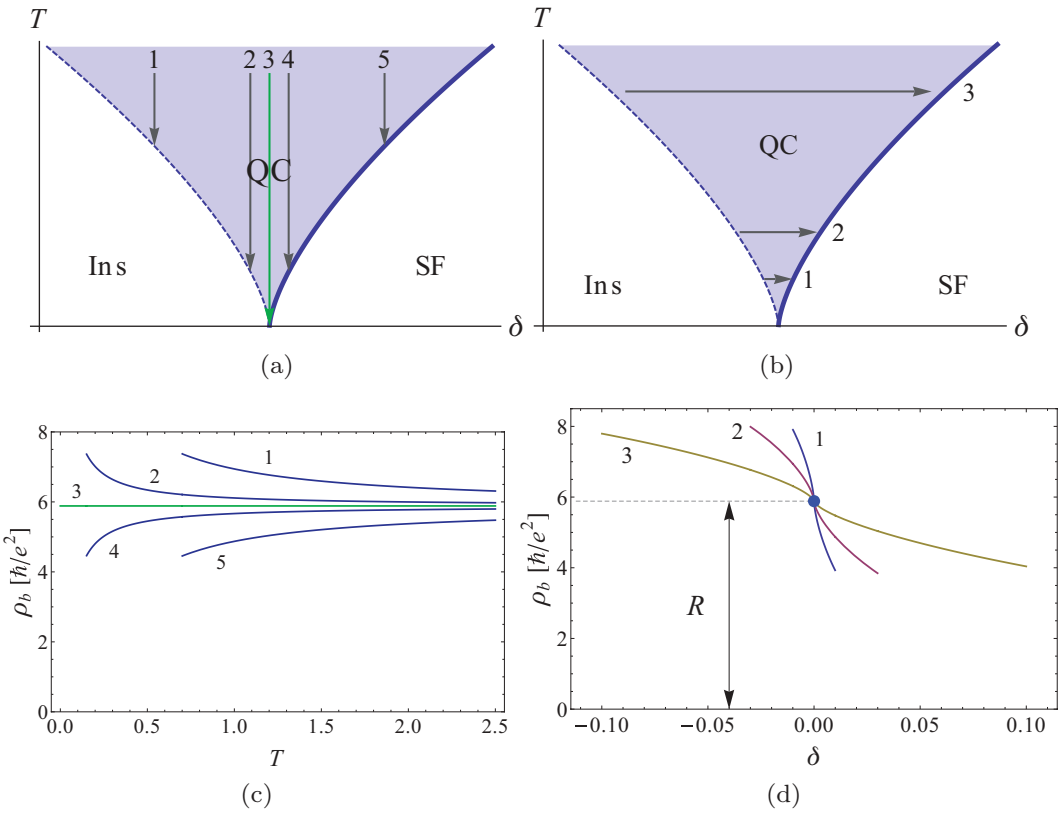

FIG. 15. (Color online) Behavior of the low-temperature dc resistivity near the quantum critical (QC) superfluid–Mott-insulator phase transition. In (a) and (b), the solid line delimiting the SF indicates a Kosterlitz-Thouless transition. Panel (c) shows the resistivity vs T for different ratios of the nonthermal parameter δ, which would tune the onsite repulsion U over the tunneling amplitude t in a Bose-Hubbard model, for example. The corresponding cuts are shown in the phase diagram in (a) and correspond to $\delta = -0.01, -0.001, 0, 0.001, 0.01$ going from curve 1 to 5. Panel (d) shows the resistivity vs δ at different temperatures, with the corresponding cuts shown in the phase diagram in (b). Curves 1,2,3 correspond to $T = 0.5, 1.0, 2.5$, respectively. The universal resistivity at criticality is $\rho_b = R\hbar/e^2$, with $R = 5.88$. (δ and T are given in a common and arbitrary unit of energy.)

quartic interaction:

$$I_{\pm} = -\frac{2u^2}{9}\int\prod_{i=1}^{3}\frac{d^2\boldsymbol{k}_i}{(2\pi)^d 2\epsilon_{k_i}}(\mathcal{F}_{\pm}^{\text{out}} - \mathcal{F}_{\pm}^{\text{in}})\frac{(2\pi)^{d+1}}{2\epsilon_k} \times \delta(\boldsymbol{k}+\boldsymbol{k}_1-\boldsymbol{k}_2-\boldsymbol{k}_3)\delta(\epsilon+\epsilon_{k_1}-\epsilon_{k_2}-\epsilon_{k_3}), \quad \text{(B3)}$$

where scattering processes out of state $\{\boldsymbol{k},\pm\}$ have

$$\mathcal{F}_{\pm}^{\text{out}} = 2f_{\pm}(\boldsymbol{k})f_{\mp}(\boldsymbol{k}_1)[1+f_{\pm}(\boldsymbol{k}_2)][1+f_{\mp}(\boldsymbol{k}_3)] + f_{\pm}(\boldsymbol{k})f_{\pm}(\boldsymbol{k}_1)[1+f_{\pm}(\boldsymbol{k}_2)][1+f_{\pm}(\boldsymbol{k}_3)], \quad \text{(B4)}$$

$\mathcal{F}_{\pm}^{\text{in}}$ is obtained by interchanging $f_{\pm}$ and $1+f_{\pm}$. We now linearize the QBE to linear order in the temperature gradient. From the left-hand side,

$$\frac{\partial f_{\pm}}{\partial \boldsymbol{x}} = -\epsilon_k \partial_{\epsilon_k} n(\epsilon_k)\frac{\boldsymbol{\nabla} T}{T}, \quad \text{(B5)}$$

while the expanded distribution function reads as

$$f_{\pm}(\boldsymbol{k}) = n(\epsilon_k) + \boldsymbol{k}\cdot\frac{\boldsymbol{\nabla} T}{T}\phi(k), \quad \text{(B6)}$$

with ϕ characterizing the departure from equilibrium due to the applied thermal gradient; it is analogous to φ used above in the context of electric transport. An important difference is that the thermal gradient leads to the same nonequilibrium distribution functions for both the positive and negative charge excitations: $f_+ = f_-$, contrary to the case with an electric field. In the linear-response regime, the heat current is simply the energy current:

$$\boldsymbol{J}_h = \int_{\boldsymbol{k}} \boldsymbol{v}_k \epsilon_k [f_+(\boldsymbol{k}) + f_-(\boldsymbol{k})] = 2\frac{\boldsymbol{\nabla} T}{T}\int_{\boldsymbol{k}} k_x^2 \phi(k), \quad \text{(B7)}$$

while we naturally get a vanishing electric current because the latter involves the integral of $f_+(\boldsymbol{k}) - f_-(\boldsymbol{k})$ [see Eq. (35)]. This is as it should be since the thermal conductivity is measured in an open circuit setup in which there is no electric charge flow in the steady state.

The linearized QBE reads as

$$-\partial_k n_k = I[\phi(k)], \quad \text{(B8)}$$

where the functional for the linearized collision integral is

$$I[\phi(k)] = -\frac{\pi\varepsilon^2}{75k^4}\left\{\frac{18k^2\phi_k}{n_k}\int dk_1 dk_2\, I_1(k,k_1,k_2) n_{k_1} n_{k_2} \times (1+n_{k_2+k_1-k}) \right. \quad \text{(B9)}$$

$$-6(1+n_k)\int dk_1 dk_2 \frac{\phi_{k_1}}{n_{k_1}} I_2(k,k_1,k_2) n_{k_2} n_{k+k_1-k_2} \quad \text{(B10)}$$

$$-12 n_k \int dk_1 dk_2 \frac{\phi_{k_1}}{n_{k_1}} I_3(k,k_1,k_2) n_{k_2}\left(1+n_{k_2+k-k_1}\right)\Big\}. \quad \text{(B11)}$$

The functions I_i result from the angle and k_3 angle integrations of the δ functions and are given in Ref. 22. We are using the shorthand $n_k = n(k)$, having dropped the mass $\mathcal{O}(\sqrt{\varepsilon})$ in the dispersion relation $\epsilon_k = \sqrt{k^2+m^2} \approx k$ to leading order in ε.

By conformal invariance, we expect the thermal conductivity, which is given by an integral over ϕ, to be infinite as explained in Sec. VII. If we could invert the linear functional $I[\phi]$, we would obtain $\phi(k) = I^{-1}[-\partial_k n_k]$, yielding a finite function $\phi(k)$, as is the case for the electric conductivity. This would in turn imply a finite thermal conductivity, running against general symmetry arguments. In fact, $I[\phi]$ can not be inverted. In other words, the linearized scattering integral has a zero mode, i.e., a zero eigenvalue eigenfunction $\phi_0(k)$ such that $I[\phi_0(k)] = 0$. This zero mode turns out to be the left-hand side of the linearized QBE:

$$\phi_0(k) = -\partial_k n_k = n_k(1+n_k), \quad \text{(B12)}$$

as we have verified by direct substitution. Hence, the equation has no solution, or formally $\phi = \infty$, which implies that the CFT describing the Wilson-Fisher fixed point has infinite thermal conductivity. It is an excellent check on the formalism, as it is *a priori* not obvious how this divergence would come about within the QBE framework.

2. Thermal response of gauged $O(2)$ model

Let us now return to the case of relevance for the QC Mott transition. In that case, the rotors are coupled to a damped gauge field. As was explained in the main body, only the static gauge fluctuations are effective at scattering the rotor excitations. These provide a simple elastic scattering term to the QBE:

$$-\partial_k n_k = \tilde{I}[\phi(k)], \quad \tilde{I}[\phi] = I[\phi] - \frac{\phi}{\tau_a}. \quad \text{(B13)}$$

Although I itself is not invertible, $\tilde{I}$ is for any finite value of the scattering time τ_a. In particular, the zero mode of I no longer is one for $\tilde{I}$: $\tilde{I}[-\partial_k n_k] = \partial_k n_k/\tau_a$, i.e., it now has eigenvalue $-1/\tau_a$.

We have solved the QBE [Eq. (B13)] numerically and have verified the presence of a singularity when the gauge scattering rate is absent. (For simplicity, we have used a momentum-independent scattering rate, but the same conclusions will hold generically.) More precisely, the numerics yield a very large value of $\kappa/T \sim 7\times 10^4$ in the CFT limit, i.e., when $1/\tau_a = 0$. This value grows as we increase the number of Chebyshev polynomials used to expand ϕ suggesting a divergence in the limit where an infinite number of basis polynomials is used. Moreover, it becomes $\mathcal{O}(1)$ even for very small values of $1/\tau_a$, consistent with the fact that the gauge scattering rate moves the system away from the conformal point, thus rendering the thermal conductivity finite.

3. Similarity with fermionic CFT of Dirac fermions

A similar analysis of conformal zero modes in the context of thermal transport in a fermionic CFT of Dirac fermions was performed in Ref. 42. A zero mode was identified in the corresponding linearized QBE, the analog of Eq. (B8). It was was found that the zero mode is essentially given by $\phi_0(k) = -\partial_k n_F(k) = n_F(k)[1-n_F(k)]$, where n_F is the Fermi-Dirac distribution. This is the fermionic analog of the bosonic mode obtained above [Eq. (B12)]. It was further found that the introduction of anisotropy for the Dirac fermions breaks conformal invariance and makes the zero mode massive. As such, the anisotropy can be seen as the analog of the gauge scattering rate in our case.

APPENDIX C: ROTOR CURRENT POLARIZATION FUNCTION

The static, nonregularized rotor current polarization function is obtained from

$$\Pi_b^{\mathrm{j}}(0,q) = -T\sum_n \int \frac{d^2\boldsymbol{p}}{(2\pi)^2} \frac{(2\hat{q}\times\boldsymbol{p})^2}{\omega_n^2+\epsilon_p^2} \frac{1}{\omega_n^2+\epsilon_{p+q}^2}, \quad \text{(C1)}$$

where $\epsilon_p = \sqrt{p^2+m^2}$ is the rotor energy. Note the presence of a factor of 4 due to the (squared) vertex between the transverse component of the gauge field and the rotor current. Performing the Matsubara sum, we obtain

$$\Pi_b^{\mathrm{j}}(0,q) = \int \frac{d^2\boldsymbol{p}}{(2\pi)^2} \frac{1}{2} \frac{(2\hat{q}\times\boldsymbol{p})^2}{\epsilon_{p+q}^2-\epsilon_p^2} \times\left[\frac{1+2n(\epsilon_{p+q})}{\epsilon_{p+q}} - \frac{1+2n(\epsilon_p)}{\epsilon_p}\right]. \quad \text{(C2)}$$

This integral is UV divergent; putting a cutoff would lead to $\Pi_b^{\mathrm{j}}(0,0) \neq 0$, which would violate the U(1) gauge invariance. We regulate by subtracting the integrand evaluated at $q = 0$. Slight care must be used in doing so because of an undetermined limit $0/0$. The regulated expression reads as

$$\Pi_b^{\mathrm{j}}(0,q) = 2\int \frac{d^2\boldsymbol{p}}{(2\pi)^2} (\hat{q}\times\boldsymbol{p})^2 \Big\{ \frac{1}{\epsilon_{p+q}^2-\epsilon_p^2}\left[\frac{1+2n(\epsilon_{p+q})}{\epsilon_{p+q}} - \frac{1+2n(\epsilon_p)}{\epsilon_p}\right] + \frac{1}{2\epsilon_p^3}[1+2n(\epsilon_p) - \epsilon_p n'(\epsilon_p)]\Big\}, \quad \text{(C3)}$$

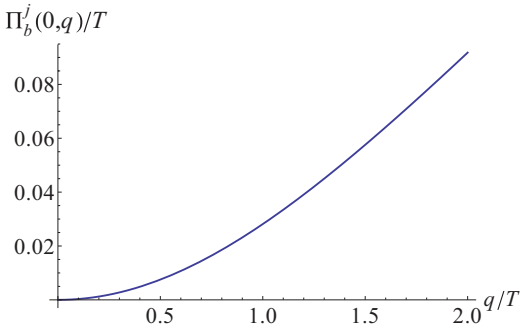

FIG. 16. (Color online) Rotor current polarization function at $\delta = 0$ so that the rotor mass is $m = \Theta T$. At small q, $\Pi_b^{\mathrm{j}} \sim q^2$, while for $q > T$, it is linear.

where $n'(\epsilon) = \partial_\epsilon n(\epsilon)$. This integral can be evaluated numerically and the result is plotted in Fig. 16. As expected, for $q \gg T$ the polarization function scales like q, as in that regime the mass ($\sim T$) is negligible and we recover the zero-temperature behavior. At small q, we obtain a q^2 scaling, consistent with the diamagnetic response of massive bosons.

We can numerically extract the slope of the polarization function at large q/T to obtain the result quoted in Eq. (18), i.e., $\sigma_b^\infty \approx 0.063$. This corresponds to the rotor conductivity in the $\omega/T \gg 1$ limit, and agrees with the analytic expression $1/16 = 0.0625$ given in Sec. VI A.

[1] M. Imada, A. Fujimori, and Y. Tokura, Rev. Mod. Phys. **70**, 1039 (1998).
[2] S. Florens and A. Georges, Phys. Rev. B **70**, 035114 (2004).
[3] S.-S. Lee and P. A. Lee, Phys. Rev. Lett. **95**, 036403 (2005).
[4] T. Senthil, Phys. Rev. B **78**, 035103 (2008).
[5] T. Senthil, Phys. Rev. B **78**, 045109 (2008).
[6] D. Podolsky, A. Paramekanti, Y. B. Kim, and T. Senthil, Phys. Rev. Lett. **102**, 186401 (2009).
[7] A. C. Potter, M. Barkeshli, J. McGreevy, and T. Senthil, Phys. Rev. Lett. **109**, 077205 (2012).
[8] R. Nandkishore, M. A. Metlitski, and T. Senthil, Phys. Rev. B **86**, 045128 (2012).
[9] P. Anderson, Mater. Res. Bull. **8**, 153 (1973).
[10] Y. Shimizu, K. Miyagawa, K. Kanoda, M. Maesato, and G. Saito, Phys. Rev. Lett. **91**, 107001 (2003).
[11] S. Yamashita, T. Yamamoto, Y. Nakazawa, M. Tamura, and R. Kato, Nat. Commun. **2**, 275 (2011).
[12] T. Itou, A. Oyamada, S. Maegawa, M. Tamura, and R. Kato, Phys. Rev. B **77**, 104413 (2008).
[13] S. Yamashita, Y. Nakazawa, M. Oguni, Y. Oshima, H. Nojiri, Y. Shimizu, K. Miyagawa, and K. Kanoda, Nat. Phys. **4**, 459 (2008).
[14] M. Yamashita, N. Nakata, Y. Kasahara, T. Sasaki, N. Yoneyama, N. Kobayashi, S. Fujimoto, T. Shibauchi, and Y. Matsuda, Nat. Phys. **5**, 44 (2008).
[15] K. Kanoda and R. Kato, Annu. Rev. Condens. Matter Phys. **2**, 167 (2011).
[16] Y. Okamoto, M. Nohara, H. Aruga-Katori, and H. Takagi, Phys. Rev. Lett. **99**, 137207 (2007).
[17] Y. Kurosaki, Y. Shimizu, K. Miyagawa, K. Kanoda, and G. Saito, Phys. Rev. Lett. **95**, 177001 (2005).
[18] O. I. Motrunich, Phys. Rev. B **72**, 045105 (2005).
[19] D. N. Sheng, O. I. Motrunich, and M. P. A. Fisher, Phys. Rev. B **79**, 205112 (2009); M. S. Block, D. N. Sheng, O. I. Motrunich, and M. P. A. Fisher, Phys. Rev. Lett. **106**, 157202 (2011).
[20] T. Senthil, M. Vojta, and S. Sachdev, Phys. Rev. B **69**, 035111 (2004).
[21] S. Sachdev, *Quantum Phase Transitions*, 2nd ed. (Cambridge University Press, Cambridge, England, 2011).
[22] K. Damle and S. Sachdev, Phys. Rev. B **56**, 8714 (1997).
[23] S.-S. Lee, Phys. Rev. B **80**, 165102 (2009).
[24] C. Nayak and F. Wilczek, Nucl. Phys. B **417**, 359 (1994).
[25] D. F. Mross, J. McGreevy, H. Liu, and T. Senthil, Phys. Rev. B **82**, 045121 (2010).
[26] R. K. Kaul, M. A. Metlitski, S. Sachdev, and C. Xu, Phys. Rev. B **78**, 045110 (2008).
[27] L. B. Ioffe and A. I. Larkin, Phys. Rev. B **39**, 8988 (1989).
[28] M.-C. Cha, M. P. A. Fisher, S. M. Girvin, M. Wallin, and A. P. Young, Phys. Rev. B **44**, 6883 (1991).
[29] S. Sachdev, Phys. Rev. B **57**, 7157 (1998).
[30] W. Witczak-Krempa and S. Sachdev, arXiv:1210.4166 [Phys. Rev. B (to be published)].
[31] A. V. Chubukov, S. Sachdev, and J. Ye, Phys. Rev. B **49**, 11919 (1994).
[32] P. A. Lee and N. Nagaosa, Phys. Rev. B **46**, 5621 (1992).
[33] Y. B. Kim, P. A. Lee, and X.-G. Wen, Phys. Rev. B **52**, 17275 (1995).
[34] C. P. Nave and P. A. Lee, Phys. Rev. B **76**, 235124 (2007).
[35] T. Senthil (unpublished).
[36] M. Vojta, Y. Zhang, and S. Sachdev, Int. J. Mod. Phys. B **14**, 3719 (2000).
[37] G. Pálsson and G. Kotliar, Phys. Rev. Lett. **80**, 4775 (1998).
[38] K. Kanoda *et al.* (unpublished).
[39] R. Kato *et al.* (unpublished).
[40] M. J. Bhaseen, A. G. Green, and S. L. Sondhi, Phys. Rev. Lett. **98**, 166801 (2007).
[41] M. J. Bhaseen, A. G. Green, and S. L. Sondhi, Phys. Rev. B **79**, 094502 (2009).
[42] L. Fritz and S. Sachdev, Phys. Rev. B **80**, 144503 (2009).